Hindawi
Wireless Communications and Mobile Computing
Volume 2022, Article ID 5001662, 23 pages
https://doi.org/10.1155/2022/5001662

Research Article

Monitoring Area Coverage Based on Adjusting Node Spacing in Mixed Underwater Mobile Wireless Sensor Networks

Qiangyi Li[1,2,3] **and Ningzhong Liu**[1,2,3]

[1]*College of Computer Science and Technology, Nanjing University of Aeronautics and Astronautics, Nanjing, 211106 Jiangsu, China*
[2]*MIIT Key Laboratory of Pattern Analysis and Machine Intelligence, Nanjing, 211106 Jiangsu, China*
[3]*Collaborative Innovation Center of Novel Software Technology and Industrialization, Nanjing, 211106 Jiangsu, China*

Correspondence should be addressed to Qiangyi Li; l@nuaa.edu.cn and Ningzhong Liu; lnznuaa@126.com

Received 11 April 2022; Revised 2 July 2022; Accepted 30 September 2022; Published 4 November 2022

Academic Editor: Rahim Khan

Wireless sensor nodes have the characteristics of small size, light weight, simple structure, and limited energy. They are random during deployment in the monitoring area, and the location of nodes is uncertain after deployment. It is easy to have uneven node distribution, resulting in dense nodes in some areas and sparse nodes in some areas. In the area with dense nodes, the monitoring area is covered repeatedly due to the distance between nodes which is too close. In the area with sparse nodes, the problem of covering blind areas appears due to the distance between nodes which is too far. Aiming at the complex structure of underwater wireless sensor networks, a coverage algorithm based on adjusting the nodes spacing is proposed. The algorithm calculates the reasonable distance between adjacent nodes before the wireless sensor node moves. The distance between wireless sensor nodes increases gradually. The simulation results show that the algorithm can make the clustered wireless sensor nodes disperse gradually by reasonably adjusting the distance between wireless sensor nodes, improve the coverage effect of wireless sensor networks, and reduce the energy consumption of wireless sensor nodes.

1. Introduction

Most of the existing coverage algorithms for wireless sensor networks are to solve various problems in the two-dimensional network environment [1]. The existing node deployment algorithms of underwater wireless sensor networks, including sea surface, seabed, and ocean node deployment, are studied and analyzed [2]. Summarize the advantages and disadvantages of existing node deployment algorithms for underwater wireless sensor networks. At present, the node deployment of underwater wireless sensor networks mainly focuses on the research of node deployment based on underwater acoustic communication [3]. Underwater acoustic communication has its own inherent shortcomings, such as low communication bandwidth and long delay time [4]. A basic problem of mobile wireless sensor networks is to improve the coverage of the monitoring area [5]. The quality of service of mobile wireless sensor networks depends on the coverage effect of the monitoring area, network connectivity, and data processing ability of mobile wireless sensor networks [6]. Each wireless sensor node may be in the working, sleeping, relay, idle, or fault state in its life cycle.

The most important difference between underwater wireless sensor networks and terrestrial sensor networks is the use of different communication transmission media [7]. Underwater communication is transmitted through underwater acoustic channels, while on the ground, it is transmitted through electromagnetic waves [8]. Underwater acoustic communication channel has serious attenuation and delay, which is easy to produce underwater ranging error, which has a great impact on the positioning of underwater wireless sensor nodes [9]. Underwater wireless sensor nodes are easily affected by

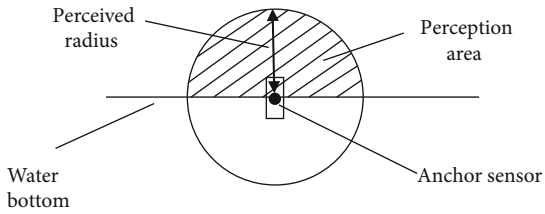

Figure 1: Perception effect of anchor sensor.

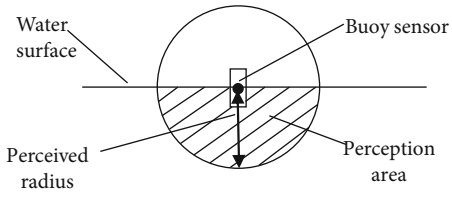

Figure 2: Perception effect of buoy sensor.

water flow and other factors, and the movement of nodes is usually unpredictable, which leads to rapid changes in the location coordinates of nodes [10]. Because the node coordinates are not easy to determine, it will affect the effective coverage of the node to the sensing area [11]. Underwater wireless sensor nodes usually add more sensing devices and some underwater transceiver devices in hardware design, which increases the cost of underwater sensor devices [12]. There are many chemical components in seawater, and the node design needs to consider the waterproof and corrosion-resistant functions [13]. Compared with ground wireless sensor nodes, underwater wireless sensor nodes are more expensive [14]. Therefore, in terms of node deployment, the deployment of underwater wireless sensor nodes is not as dense as that of ground sensor nodes, so it is more important to reasonably adjust the location of nodes. Underwater communication channel has intermittent characteristics. Underwater wireless sensor nodes need to cache data, which has certain requirements on the storage capacity of underwater sensor nodes [15]. Moreover, the computing power of wireless sensor nodes is limited, which makes underwater wireless sensor networks adopt location algorithms with less resource consumption and low complexity.

According to the problem of the underwater wireless sensor networks, a coverage algorithm based on adjusting node spacing (CA-ANS) is proposed in this article.

The main contributions of this article are as follows:

(1) The existing coverage algorithms for underwater wireless sensor networks are summarized and analyzed

(2) The problems of existing coverage algorithms for underwater wireless sensor networks are pointed out

(3) An improved coverage algorithm for underwater wireless sensor networks is proposed in this article

The main structure of this article is organized as follows:

(1) The research background is introduced in Section 1

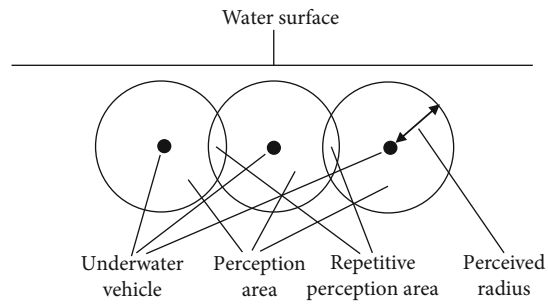

Figure 3: Perception effect of underwater vehicle.

(2) The existing related work is analyzed in Section 2

(3) This article algorithm is described in Section 3

(4) The simulation analysis is given in Section 4

(5) This article is summarized in Section 5

2. Related Work

In order to solve these problems, Priyadarshini and Sivakumar [16] proposed a new method to achieve maximum coverage and maximum connectivity in mobile underwater acoustic wireless sensor networks (MUAWSN), using the random cluster deployment of sensors in MUAWSN. In MUAWSN, the coverage blind area problem occurs because the node is damaged or the number of active nodes is lower than the threshold limit. An energy prediction algorithm is proposed, which improves the maximum coverage and connectivity of data transmission by analyzing the sample values of known parameters on the water surface. Due to the mobility of water caused by wave, wind, ocean current, network coverage, and connection performance, the topology will change. The random mobility of nodes is stretched in two-dimensional space, so as to obtain the maximum coverage and connectivity in three-dimensional space.

With the change of monitoring tasks and requirements, there will be a large number of blind areas covered by underwater monitoring, and the traditional network repair strategy cannot be applied to the changing underwater monitoring tasks and the harsh multiconstraint three-dimensional underwater environment. It is of great significance to meet the diversified monitoring needs in the harsh and dangerous three-dimensional underwater environment. Multiple autonomous underwater vehicles (multi-AUVs) have strong adaptability and flexibility in dangerous and harsh three-dimensional underwater environment. Zhuang et al. [17] proposed the repair model of underwater monitoring coverage blind area under various constraints. The multiagent event coverage hole repair (MECHR) algorithm combining multiagent strategy and diversity archiving strategy is used to repair the underwater monitoring coverage blind area in UWSNs. The algorithm completes the subtasks symmetrically through information exchange and interactive operation with other agents. The algorithm can adapt to a variety of harsh scenes and multiconstraint three-dimensional underwater environment. The effect

(1) Input: length, width, j, R_S, $(x_{R''}, y_{R''}, z_{R''})$
(2) If $d(S_A, S_B) < d_t$ then
(3) Nodes are moved according to formula (17) to formula (20)
(4) End if
(5) If $d(S_A, S_B) \geq d_t$ then
(6) Nodes do not need to be moved
(7) End if
(8) Output: The new position of the nodes

Pseudocode 1.

(1) Input: length, width, depth, k, R_S, $(x_{R'''}, y_{R'''}, z_{R'''})$
(2) If $d(S_A, S_B) < d_t$ then
(3) Underwater vehicle nodes are moved according to formula (23) to formula (28)
(4) End if
(5) If $d(S_A, S_B) \geq d_t$ then
(6) Underwater vehicle nodes do not need to be moved
(7) End if
(8) Output: The new position of underwater vehicle nodes

Pseudocode 2.

of MECHR algorithm is verified by underwater repair simulation experiment. The algorithm can adapt to the changing three-dimensional underwater monitoring environment.

The development of wireless sensor networks in smart cities shows that the deployment of wireless sensor nodes in three-dimensional space is very important, which can affect the quality of service of wireless sensor networks. With the rapid development of smart city, Priyadarshi and Gupta [18] discussed the mathematical model of maximum space coverage obtained by nonlinear optimization method in three-dimensional space and obtained the number of nodes required for the maximum monitoring area of network coverage through calculation and derivation of mathematical formula. A three-dimensional network monitoring area coverage and node deployment based on three-dimensional structure is proposed. The deterministic deployment scheme can maintain the mathematical model of monitoring area coverage effect by using a small number of nodes. The monitoring area in the network is divided into three-dimensional grids, and the nodes are deployed according to the mathematical model of wireless sensor network coverage. Compared with the traditional three-dimensional structure node deployment method and tetrahedral structure node deployment scheme, the number of nodes used in this algorithm can be less.

Yao and Du [19] mainly studied the placement strategy of underwater monitor in a complex underwater environment model to obtain the most effective deployment position after calculation. Input the three-dimensional underwater topographic map. The negative gradient direction is the fastest descent direction, a complex underwater terrain can be fitted into a differentiable function, and the minimum value of the function can be found to determine the low-lying area of the underwater terrain. The placement strategy of underwater monitor depends on the gradient direction algorithm, which solves the problem of maximum underwater coverage: find the maximum coverage set of underwater monitor in three-dimensional workspace. Using the duality principle of the maximum split subset of the cover set and the cover set, the target set is found, and finally, the suboptimal cover set is found. Compared with random deployment algorithm, this algorithm has higher network coverage quality.

Underwater wireless sensor networks (UWSNs) have been widely used in environmental monitoring, military monitoring, data acquisition, and other fields. The deployment of sensor nodes in three-dimensional underwater wireless sensor networks is a key problem, but it is a challenging problem due to the complexity of underwater environment. Yan et al. [20] proposed a growth ring nonuniform node depth adjustment self-deployment optimization algorithm to improve the coverage and reliability of UWSNs and solve the problem of energy blind area. A construction scheme of sensor node connection tree structure based on growth ring style is proposed, and a global optimal depth adjustment algorithm aiming at maximizing coverage utilization and comprehensive optimization of energy balance is proposed. Initially, the nodes are scattered on the water surface to form a connected network on this two-dimensional plane. Then, starting from the sink node, a growth ring incremental strategy is proposed, which organizes the ordinary nodes into a tree structure and determines each root of the subtree. At the same time, with the goal of maximizing global coverage utilization and energy balance, all node depths are calculated iteratively. Finally, all nodes are dived to the calculation position at one time to build a three-dimensional nonuniform distribution and energy balanced underwater connected network. A series of simulation experiments are

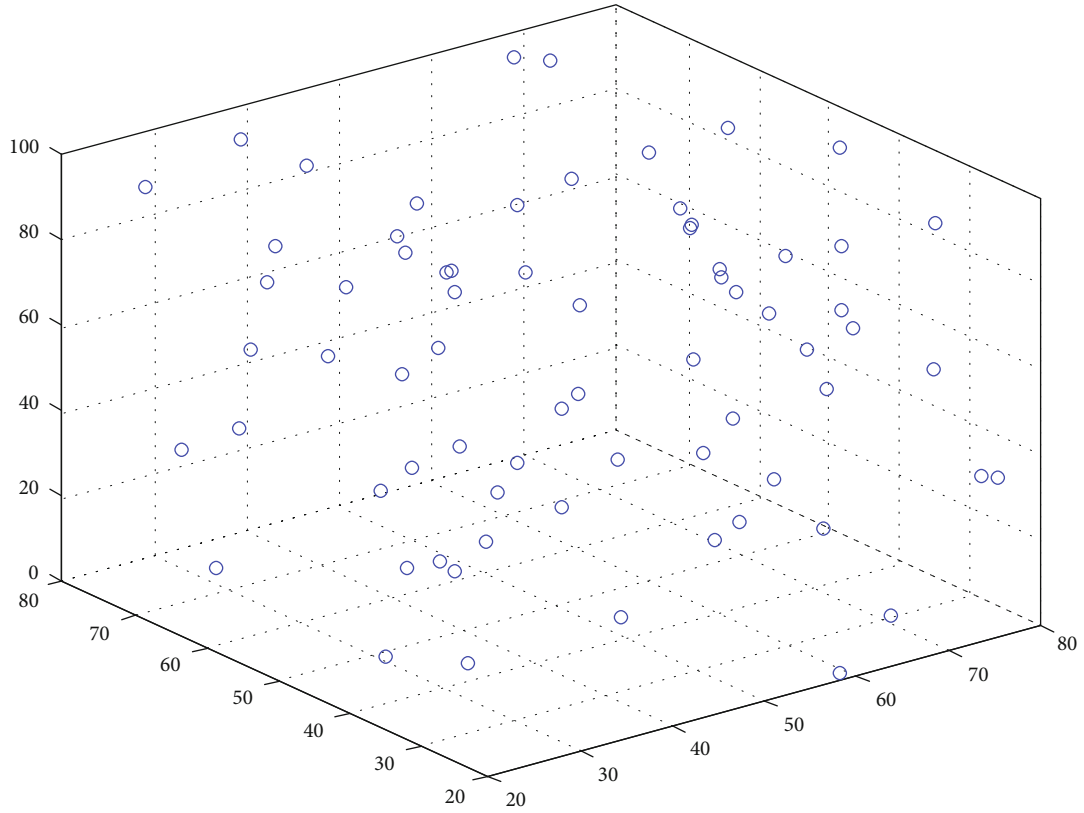

(a) Before node movement

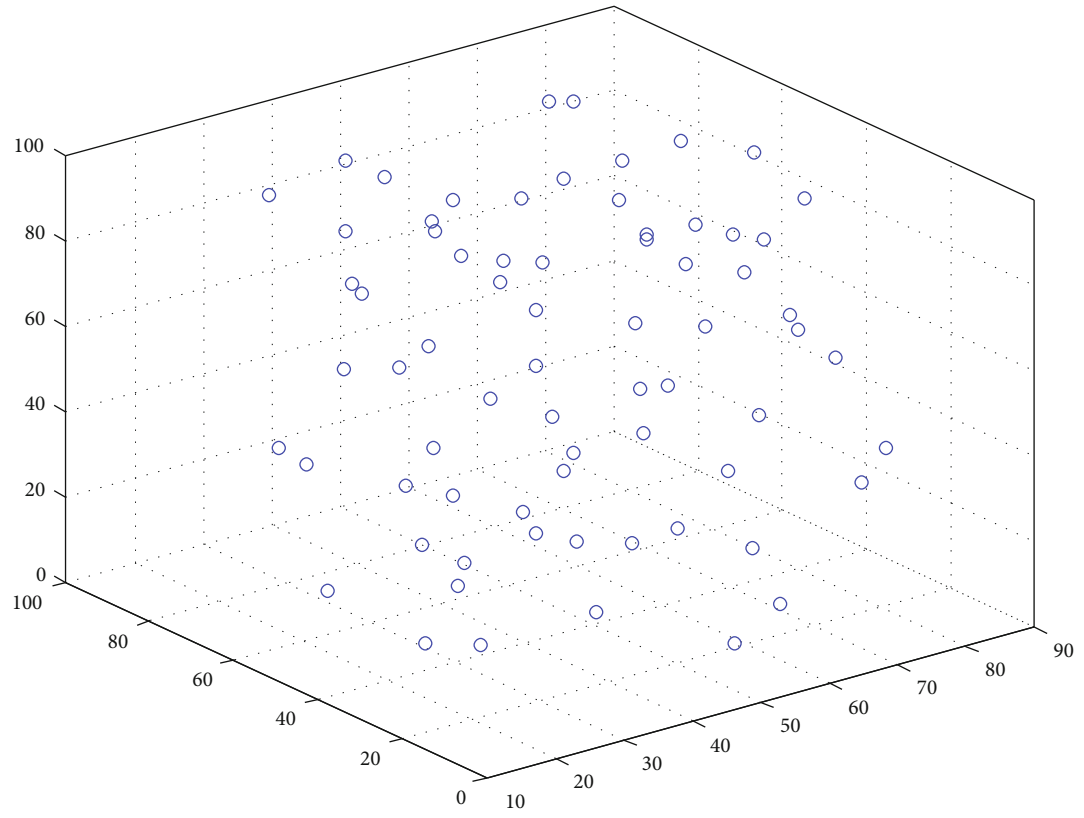

(b) After node movement

Figure 4: Coverage effect before and after node movement when the total number of nodes is 70.

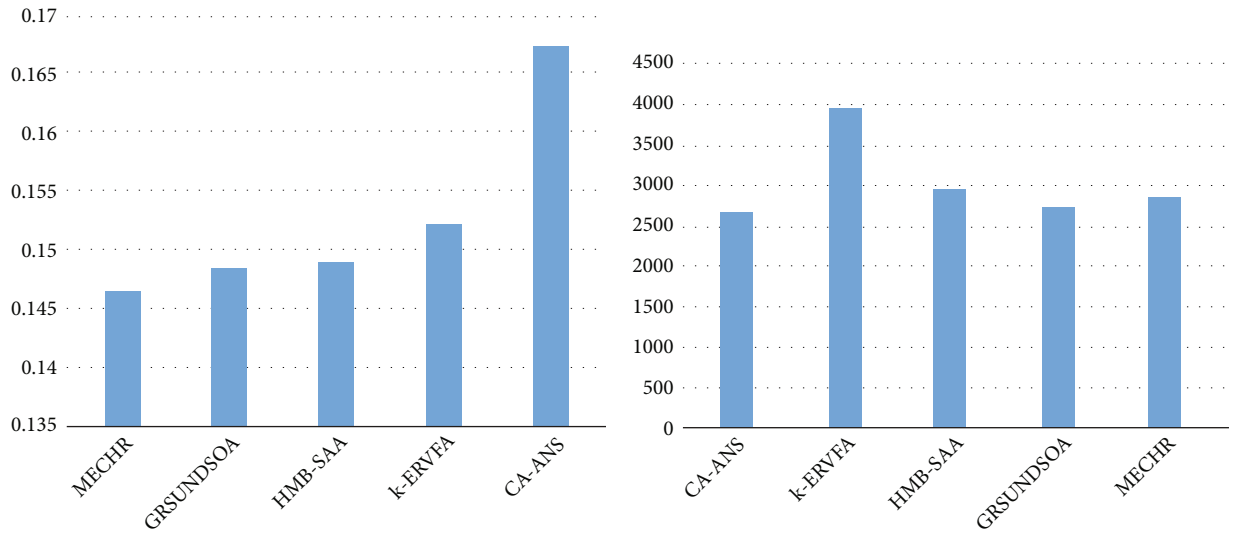

(a) Coverage effect

(b) Energy consumption

Figure 5: Coverage effect and energy consumption when the total number of nodes is 70.

carried out. The simulation results show that under the condition of full connectivity and energy balance, the coverage and reliability of UWSN are greatly improved, and the problem of energy blind area is effectively avoided. Therefore, GRSUNDSOA can significantly prolong the life of UWSN.

In underwater wireless sensor networks, topology control has attracted extensive attention. Considering the complexity of underwater environment, Zhang et al. [21] adopted the topology model of three-dimensional dense network. First, partition units, clusters, and temporary control nodes are defined, and a clustering sleep scheduling algorithm is proposed. On this basis, a vulnerability repair algorithm considering the vulnerability of sensor nodes affected by external factors is proposed. The algorithm defines fault nodes, coverage vulnerability, coverage matrix, key locations, and supplementary nodes. The algorithm also uses the coverage matrix and vulnerability edge nodes to determine whether the coverage blind area needs to be repaired.

Most of the existing fence coverage studies assume that the sensor is deployed in a two-dimensional long thin strip area, in which the fence is a sensor connection belt from one end of the area to the other end, and the sensing areas of adjacent sensors overlap each other. However, the two-dimensional assumption cannot cover all application scenarios, such as underwater wireless sensor networks. Shen et al. [22] studied the problem of weak fence K coverage in underwater wireless sensor networks. First, they analyzed how to determine that underwater wireless sensor networks can provide three-dimensional weak fence K coverage and proposed a new and effective scheme to transform the three-dimensional weak fence K coverage problem into a two-dimensional complete K coverage problem. On this basis, an effective sensor allocation algorithm is proposed to construct weak fence K coverage and minimize the total moving distance of all sensors in underwater wireless sensor networks. The simulation results verify the correctness of the analysis and show that the algorithm is better than the greedymatch algorithm.

Underwater wireless sensor networks (UWSNs) are widely used in resource exploration, pollution monitoring, tactical monitoring, and other fields. However, the complexity and diversity of underwater environment make it obviously different from terrestrial environment. In particular, the coverage requirements may be different in different underwater areas. However, due to the different coverage requirements, there is little work on the topology control of UWSNs. Therefore, Liu et al. [23] proposed two algorithms for the diversified coverage of UWSNs: (1) diversified coverage traversal algorithm, which adjusts the perception radius of nodes in turn, that is, only one node changes its perception radius in each round. (2) Diversified coverage radius increment algorithm increases the perceived radius of nodes, that is, in each round, multiple nodes can increase their perceived radius at the same time. Through mathematical analysis and simulation, the performance of tadc and riadc is analyzed. The results show that both tadc and riadc can achieve different coverage while minimizing energy consumption. In addition, tadc and riadc perform well in obtaining the best sensing radius and reducing message complexity, respectively. These advantages further show that tadc and riadc are suitable for small-scale and large-scale underwater wireless sensor networks, respectively.

Due to the limited battery capacity of sensor nodes, minimizing energy consumption is a potential research field of underwater wireless sensor networks (UWSNs). However, the existence of energy blind area and coverage blind area leads to the performance degradation of UWSNs in network lifetime and throughput. Latif et al. [24] designed a technology to overcome the shortcomings of the existing technology to solve the problem of energy blind area in depth-based routing technology. In addition to solving the problem of energy blind area, a coverage blind area repair technology

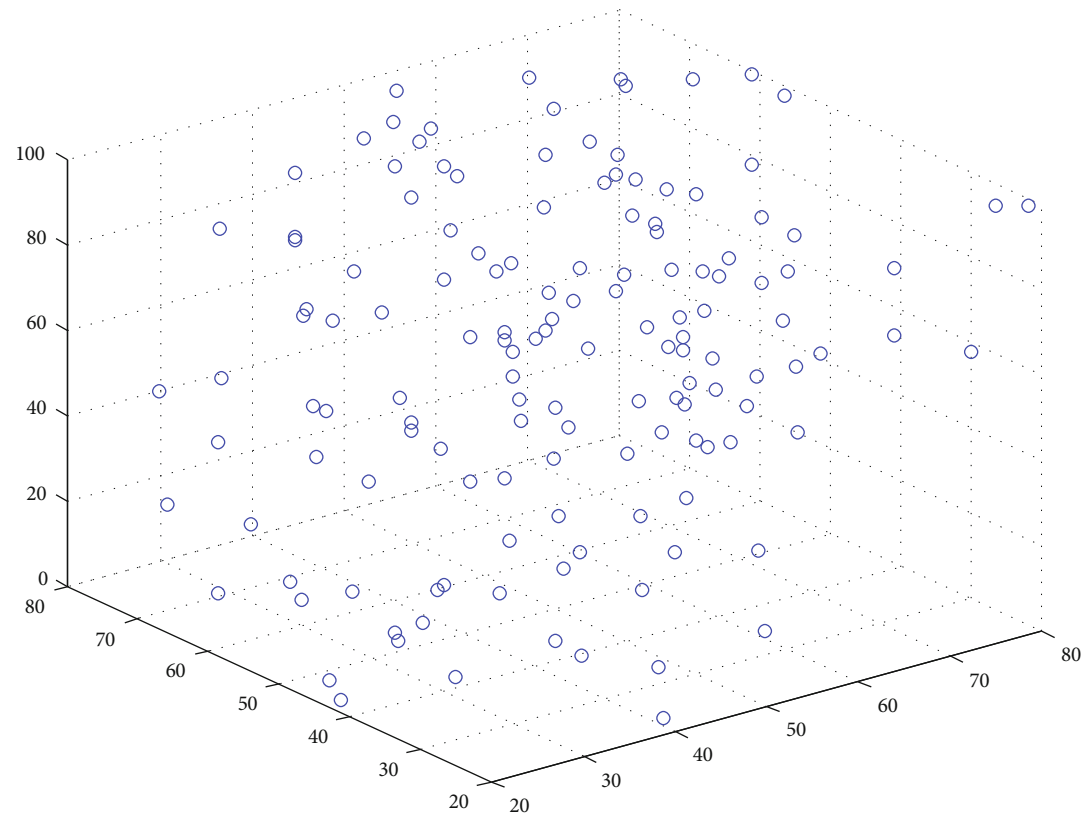

(a) Before node movement

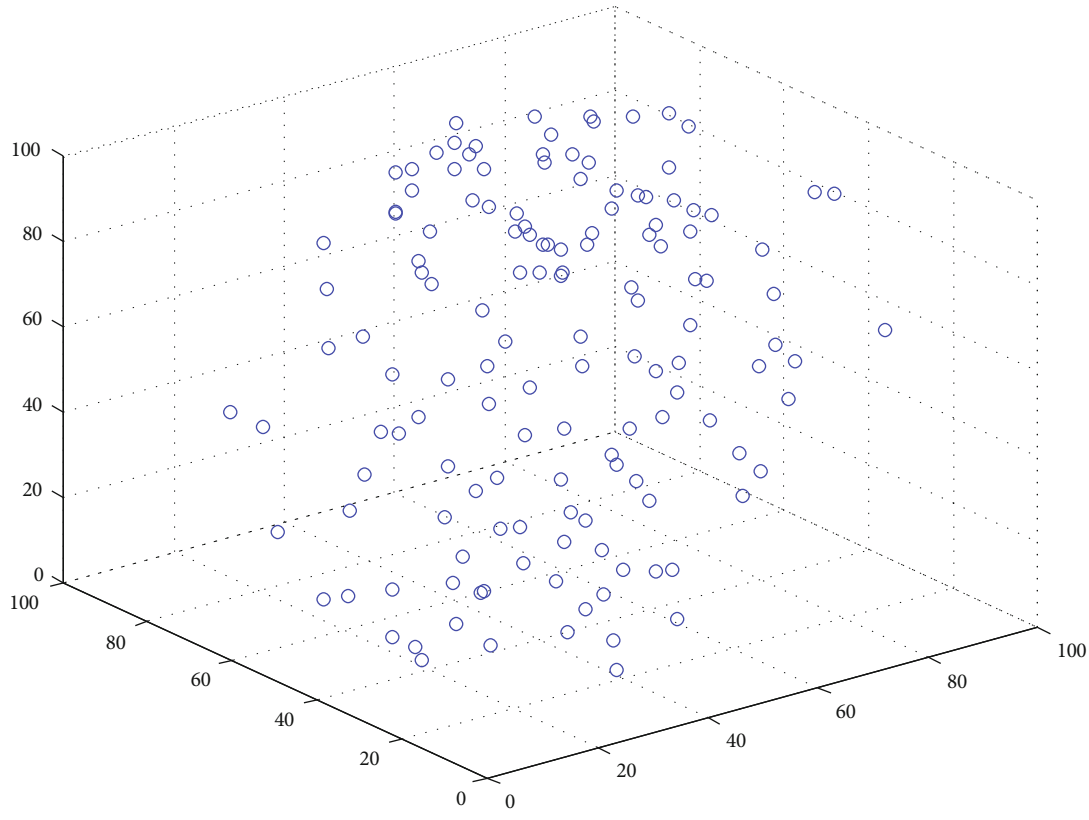

(b) After node movement

Figure 6: Coverage effect before and after node movement when the total number of nodes is 140.

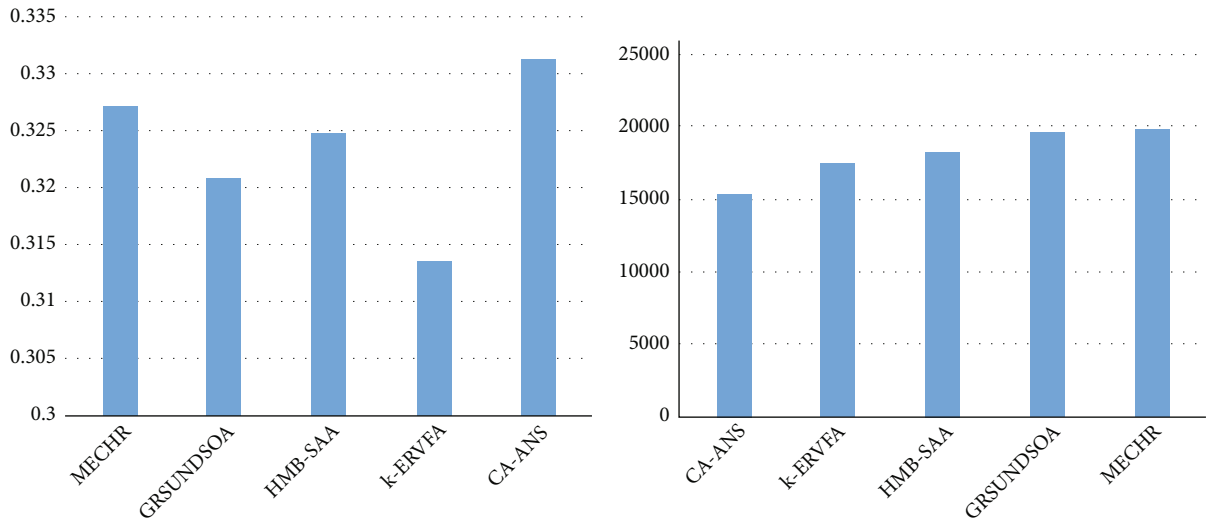

(a) Coverage effect

(b) Energy consumption

Figure 7: Coverage effect and energy consumption when the total number of nodes is 140.

is also proposed. In the dense deployment area, the perception range of nodes has redundancy and overlap. This technology makes use of the advantages of network redundancy and overlap to repair the blind area of network coverage in the process of network operation. Simulation results show that the two technologies can effectively save node energy and finally maximize the network lifetime and throughput at the cost of increasing delay.

With the extensive exploration and utilization of marine resources, the field of underwater wireless sensor networks (UWSNs) has attracted more and more attention of researchers. Due to the requirements of real-time remote data monitoring, underwater acoustic sensor network has become a preferred network to a great extent. In underwater acoustic sensor networks, the limited availability and nonrechargeability of energy resources and the relative inaccessibility of deployed sensor nodes for energy supplement make the development of a variety of energy optimization technologies necessary. Cluster is such a technology to improve system scalability and reduce energy consumption. In the unstable underwater environment, in addition to clustering, coverage and connectivity are also two important characteristics that determine the detection and communication of events of interest in underwater wireless sensor networks. Underwater communication can also use nonaudio communication technologies, such as radio frequency, magnetic induction, and underwater free space optics. Sandeep and Kumar [25] studied the clustering, coverage, and connectivity of underwater acoustic sensor networks; qualitatively compared their performance; and highlighted some key outstanding issues related to UWSNs. This article summarizes the existing clustering, coverage, and connectivity algorithms based on acoustic communication, which provides useful guidance for the research of UWSN from the perspective of other communication technologies.

The combination of wireless sensor networks (WSNs) and edge computing not only enhances its ability but also stimulates a series of new applications. As a typical application, three-dimensional underwater wireless sensor networks (UWSNs) have become a research hotspot. Wang et al. [26] first studied the minimum number of sensor nodes required to build a diversified K coverage sensor network. According to different k coverage requirements, a virtual force algorithm to enhance k coverage is proposed to realize the uneven optimization of regional coverage. The effectiveness of the algorithm is verified by theoretical analysis and simulation experiments. Detailed performance comparison shows that K-ERVFA obtains better coverage in the subregion with high k coverage, so as to realize the ideal diversified deployment of k coverage. The sensitivity of the simulation parameters is analyzed, and the K-ERVFA is extended to the sparse area and time varying situation of the sensor.

The above algorithm does not consider the problem of hybrid deployment of anchor nodes, buoy nodes, and underwater vehicles. When a large number of different types of nodes are used for mixed deployment, it can not only effectively reduce the network cost but also improve the network coverage effect in complex environment.

3. Coverage Algorithm Based on Adjusting Node Spacing

3.1. Establish Mathematical Model. There are three different types of sensors in underwater hybrid wireless sensor networks. They are the anchor sensor fixed at the bottom through the iron anchor, the buoy sensor floating on the water surface through the buoy, and the underwater vehicle that can move freely in the water.

The first type of sensor is an anchor sensor fixed at the bottom of the water through an iron anchor. This type of sensor is fixed at the bottom of the water without moving. The monitoring effect is shown in the shaded area in Figure 1.

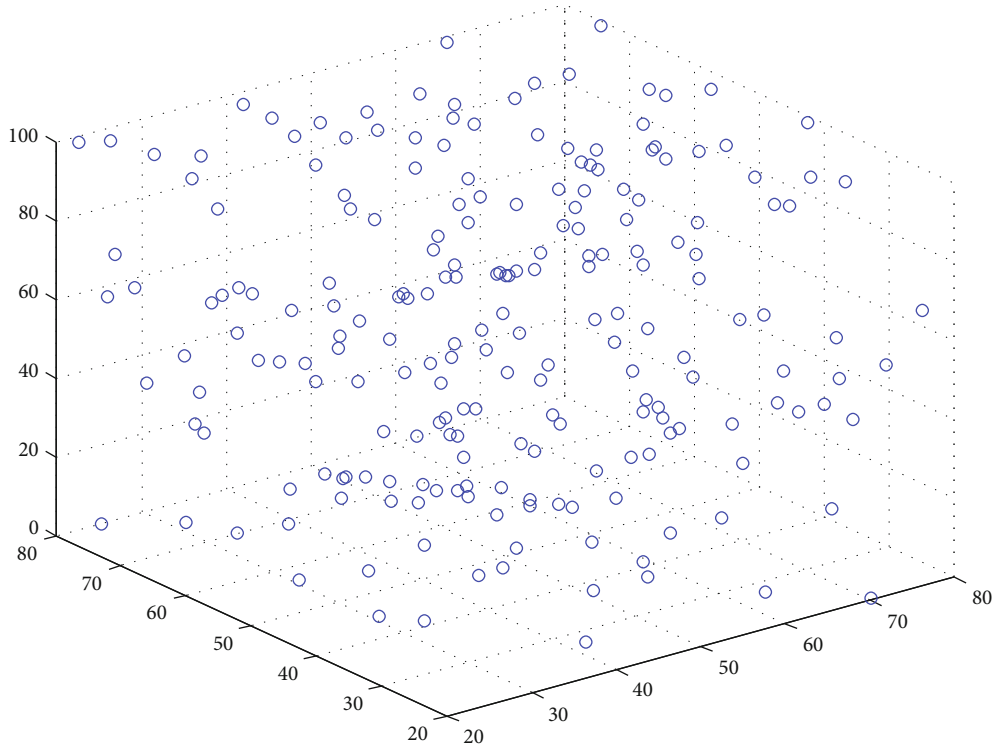

(a) Before node movement

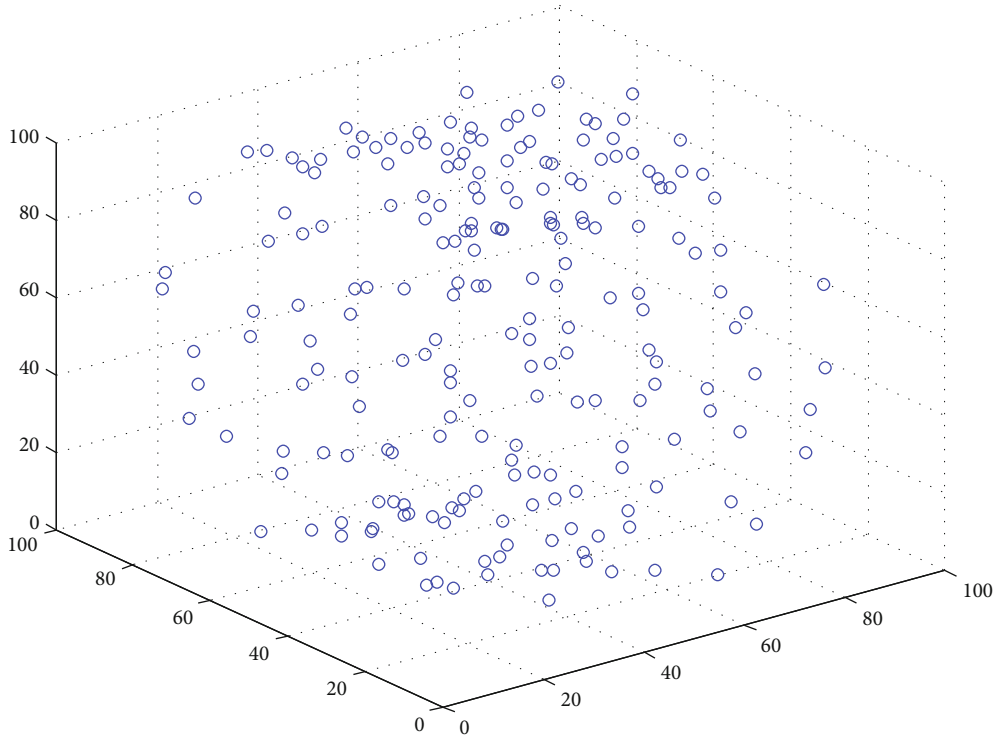

(b) After node movement

Figure 8: Coverage effect before and after node movement when the total number of nodes is 210.

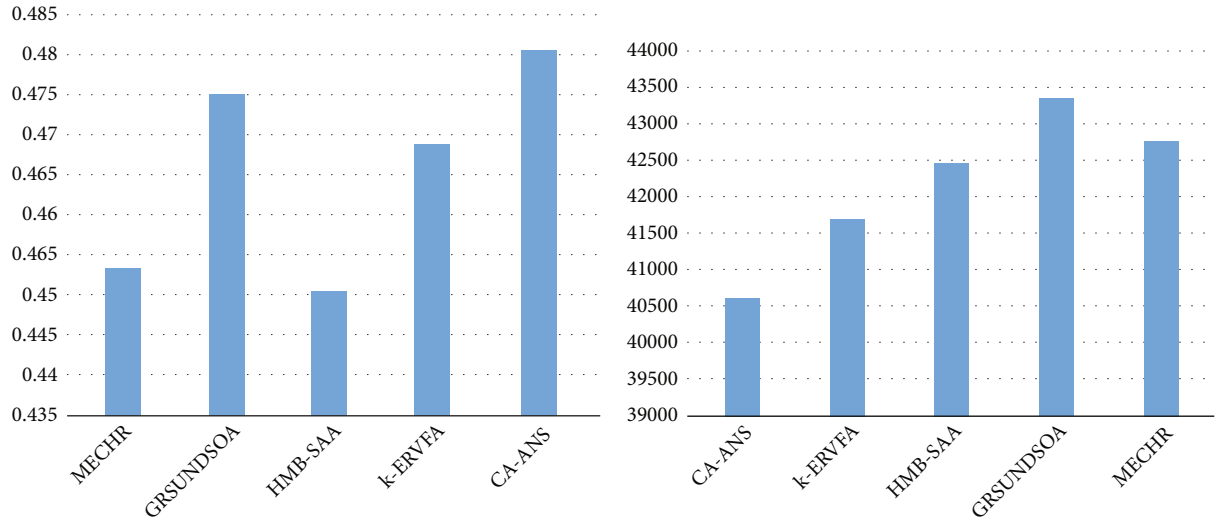

(a) Coverage effect

(b) Energy consumption

Figure 9: Coverage effect and energy consumption when the total number of nodes is 210.

The position coordinates of the first type anchored sensor node S' in the monitoring area are $(x_{R'}, y_{R'}, z_{R'})$. This type of sensor node cannot move after underwater deployment, and the position coordinates of this type of node will not change.

The second type of buoy sensor is a sensor fixed at the bottom of the water surface buoy. This type of sensor can move with the water surface buoy. The node monitoring effect is shown in the shaded area in Figure 2.

The position coordinates of the second type buoy sensor node S'' in the monitoring area are $(x_{R''}, y_{R''}, z_{R''})$. The movement of this type of sensor node can be realized through the movement of buoy, and this type of sensor node can only move along the x-axis and y-axis but cannot move along the z-axis.

The third type of sensor is an underwater vehicle that can move freely in the water. This type of sensor can move freely in the water. The node monitoring effect is shown in the shadow area in Figure 3.

The position coordinates of the third type sensor node S''' in the monitoring area are $(x_{R'''}, y_{R'''}, z_{R'''})$. The movement of this type of sensor node can be realized through the movement of underwater vehicle, and this type of sensor node can move along the x-axis, y-axis, and z-axis.

(1) Mathematical model of node binary perception

The calculation formula is as follows:

$$P(S_k, T) = \begin{cases} 0 & \text{if} \quad d(S_k, T) > R_{Sk}, \\ 1 & \text{if} \quad d(S_k, T) \le R_{Sk}. \end{cases} \tag{1}$$

In formula (1), $P(S_k, T)$ is the effect that the target point T is perceived by the kth sensor node [27].

(2) Mathematical model of node probability perception

The calculation formula is as follows:

$$P(S_k, T) = \begin{cases} 0 & \text{if} \quad d(S_k, T) > R_{Sk}, \\ \dfrac{e^{R_{Sk} - d(S_k, T)} - 1}{e^{R_{Sk}} - 1} & \text{if} \quad d(S_k, T) \le R_{Sk}. \end{cases} \tag{2}$$

In formula (2), $P(S_k, T)$ is the probability that the target point P is perceived by the kth sensor node S_k [28].

(3) Mathematical model of network coverage

The mathematical model of network coverage in the case of only one wireless sensor node is calculated as follows:

$$R_{\text{coverage}} = \frac{M_{\text{area}}}{S_{\text{area}}} = \frac{(4/3)\pi R_S^3}{L \times W \times D}. \tag{3}$$

In formula (3), the length of the monitoring area is L, the width is W, the depth is D, and the sensing radius of wireless sensor node s is R_S [29].

The mathematical model of network coverage jointly perceived by multiple nodes is calculated as follows:

$$R_{\text{coverage}} = \frac{\sum_{j=1}^{L \times W \times D/\Delta L \times \Delta W \times \Delta D} P_{\text{coverage}}(G_j)}{L \times W \times D/\Delta L \times \Delta W \times \Delta D}. \tag{4}$$

In formula (4), $\sum_{j=1}^{L \times W \times D/\Delta L \times \Delta W \times \Delta D} P_{\text{coverage}}(G_j)$ is the total number of small grids perceived by at least one wireless sensor node and $L \times W \times D/\Delta L \times \Delta W \times \Delta D$ is the total number of small grids in all monitoring areas [30].

After the first type of anchor sensor is deployed, it sinks to the bottom of the water. The coordinate of the anchor sensor S' in the monitoring area is $(x_{S_i'}, y_{S_i'}, z_{S_i'})$, $z_{S_i'} = 0$, and i is the total number of the deployed first type sensors.

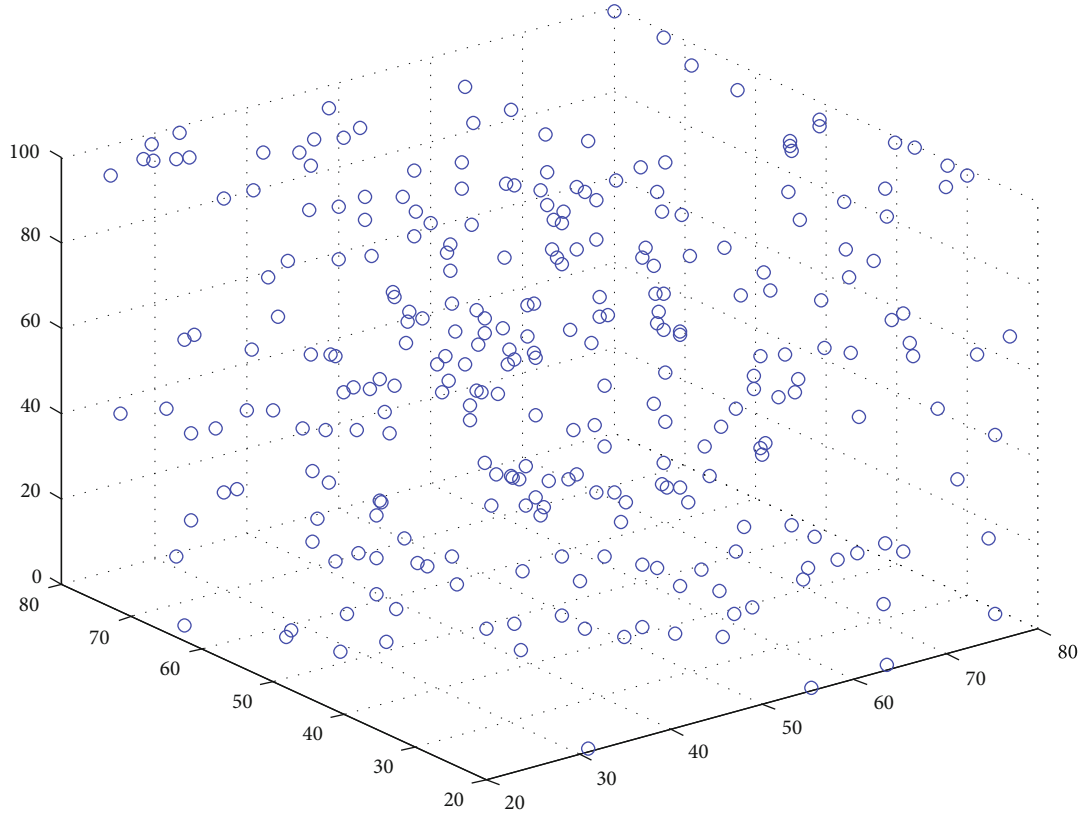

(a) Before node movement

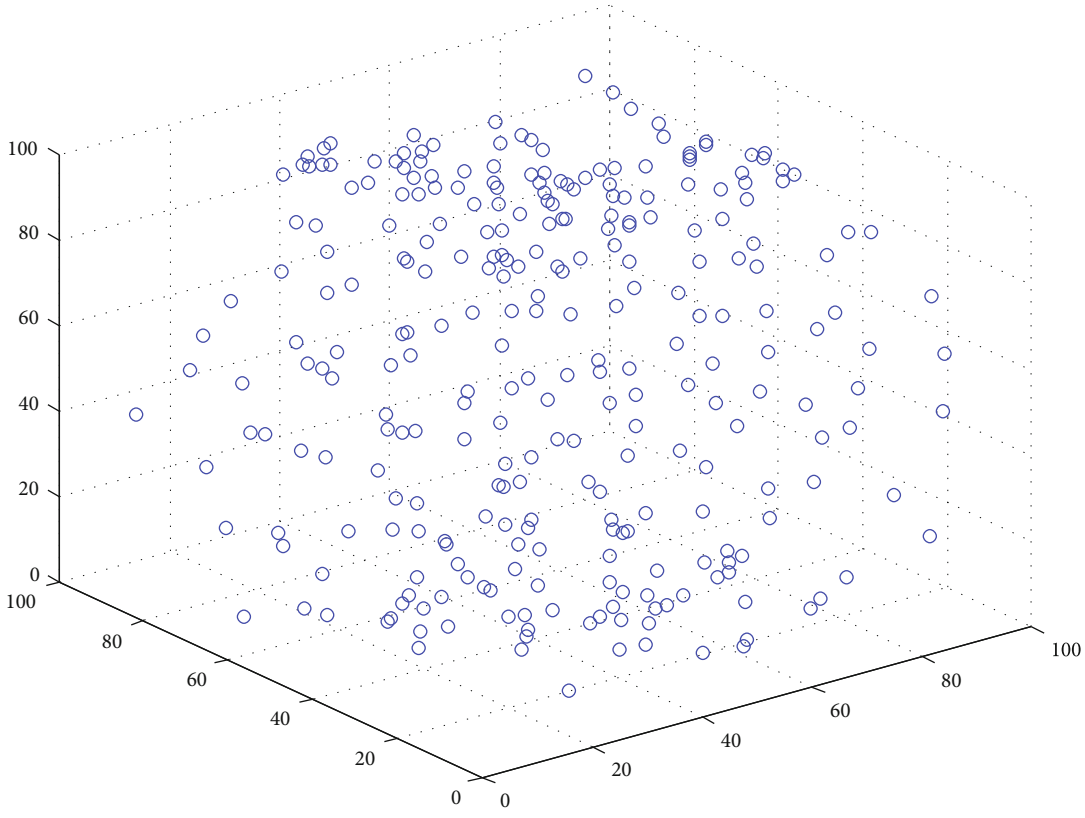

(b) After node movement

Figure 10: Coverage effect before and after node movement when the total number of nodes is 280.

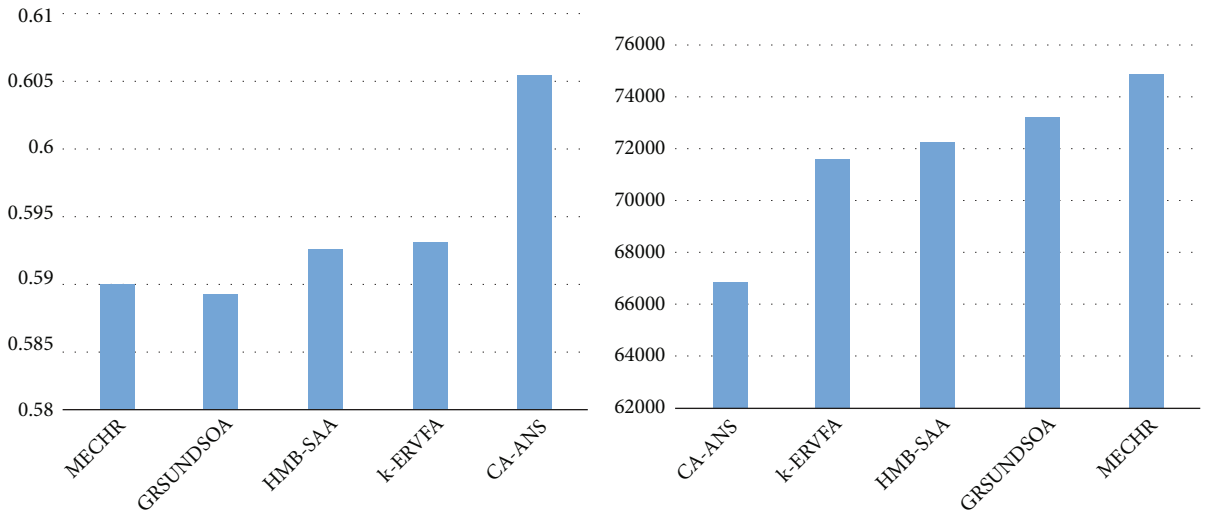

(a) Coverage effect

(b) Energy consumption

Figure 11: Coverage effect and energy consumption when the total number of nodes is 210.

After the second type of buoy sensor is deployed, it floats on the water surface. The coordinate of the buoy sensor S'' in the monitoring area is $(x_{S_i'}, y_{S_i'}, z_{S_i'})$, $z_{S_j''}$ = depth, and j is the total number of the deployed second type sensors.

After the third type of underwater vehicle is deployed, it can move freely in the water. The coordinates of the underwater vehicle S''' in the monitoring area are (x,y,z) is the total number of the deployed third type sensors.

For the first type of anchor sensor, it is fixed at the bottom of the water after deployment and cannot move, so its movement scheme is not discussed. At this time $z_{S_i'} = 0$, the coordinates of this type sensor are $(x_{S_i'}, y_{S_i'}, 0)$.

For the second type of buoy sensor, it can only move on the water surface; that is, it can only move along the x-axis direction and y-axis direction. At this time $z_{S_j''}$ = depth, the coordinates of this type sensor are $(x_{S_i'}, y_{S_i'}, \text{depth})$.

3.2. Buoy Sensor Node Spacing Calculation Process. The second type of buoy sensor can only move on the water surface, and it can be simplified as node movement in a two-dimensional plane environment. By adjusting the distance between nodes, the monitoring area of repeated coverage can be reduced and the coverage optimization of the water surface area can be realized [31].

When $d(S_A, S_B) < d_t$ the two nodes are too close, both nodes need to move.

$$d_x(S_A, S_B) = \frac{[d_t - d(S_A, S_B)](S_A^x - S_B^x)}{d(S_A, S_B)}, \tag{5}$$

$$d_y(S_A, S_B) = \frac{[d_t - d(S_A, S_B)](S_A^y - S_B^y)}{d(S_A, S_B)}, \tag{6}$$

$$d_x(S_B, S_A) = \frac{[d_t - d(S_B, S_A)](S_B^x - S_A^x)}{d(S_B, S_A)}, \tag{7}$$

$$d_y(S_B, S_A) = \frac{[d_t - d(S_B, S_A)](S_B^y - S_A^y)}{d(S_B, S_A)}. \tag{8}$$

After moving, the new coordinates of node A and node B are

$$x_{\text{new}}(S_A) = x_{\text{old}}(S_A) + d_x(S_A, S_B), \tag{9}$$

$$y_{\text{new}}(S_A) = y_{\text{old}}(S_A) + d_y(S_A, S_B), \tag{10}$$

$$x_{\text{new}}(S_B) = x_{\text{old}}(S_B) + d_x(S_B, S_A), \tag{11}$$

$$y_{\text{new}}(S_B) = y_{\text{old}}(S_B) + d_y(S_B, S_A). \tag{12}$$

When $d(S_A, S_B) \geq d_t$,

$$x_{\text{new}}(S_A) = x_{\text{old}}(S_A), \tag{13}$$

$$y_{\text{new}}(S_A) = y_{\text{old}}(S_A), \tag{14}$$

$$x_{\text{new}}(S_B) = x_{\text{old}}(S_B), \tag{15}$$

$$y_{\text{new}}(S_B) = y_{\text{old}}(S_B). \tag{16}$$

In formulas (5) to (16), $d_x(S_A, S_B)$ is that node A obtains the displacement component along the x-axis from node B.

$d_y(S_A, S_B)$ is that node A obtains the displacement component along the y-axis from node B.

$d_x(S_B, S_A)$ is that node B obtains the displacement component along the x-axis from node A.

$d_y(S_B, S_A)$ is that node B obtains the displacement component along the y-axis from node A.

d_t is the ideal distance between nodes in the tth cycle.

$d(S_A, S_B)$ is the distance between node A and node B.

$d(S_B, S_A)$ is the distance between node B and node A.

S_A^x is the position coordinates of node A on the x-axis.

S_A^y is the position coordinates of node A on the y-axis.

S_B^x is the position coordinates of node B on the x-axis.

S_B^y is the position coordinates of node B on the y-axis.

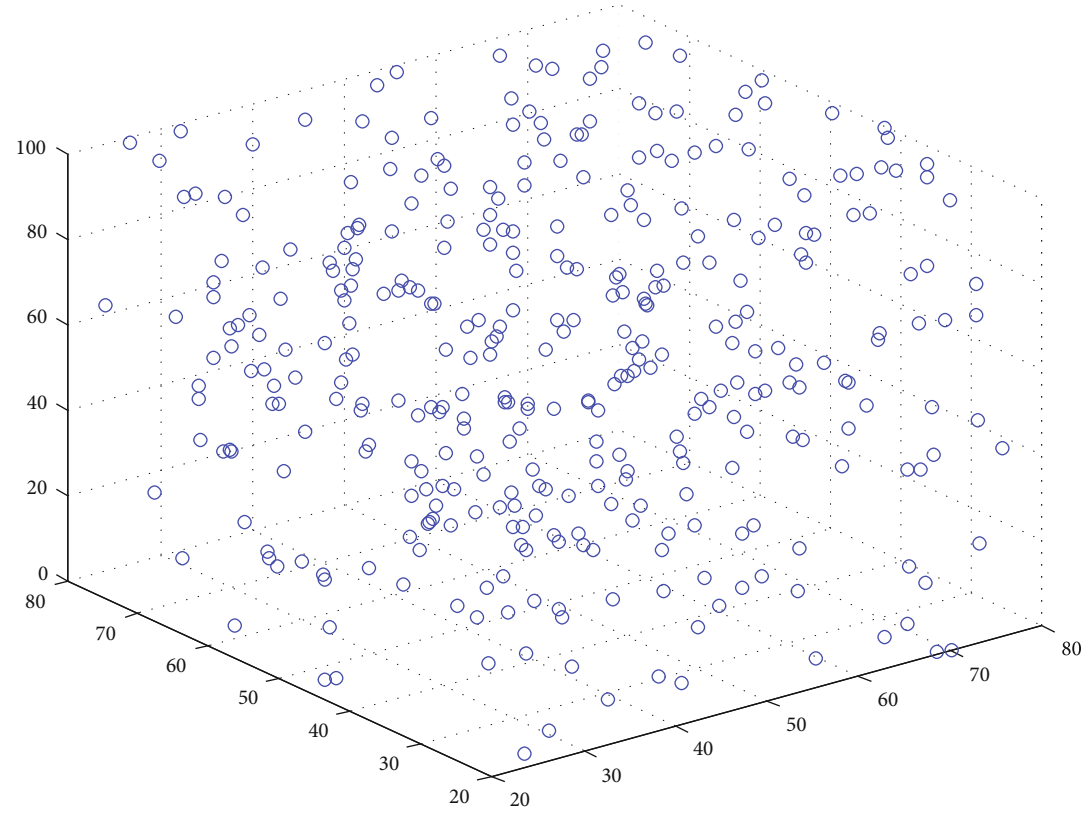

(a) Before node movement

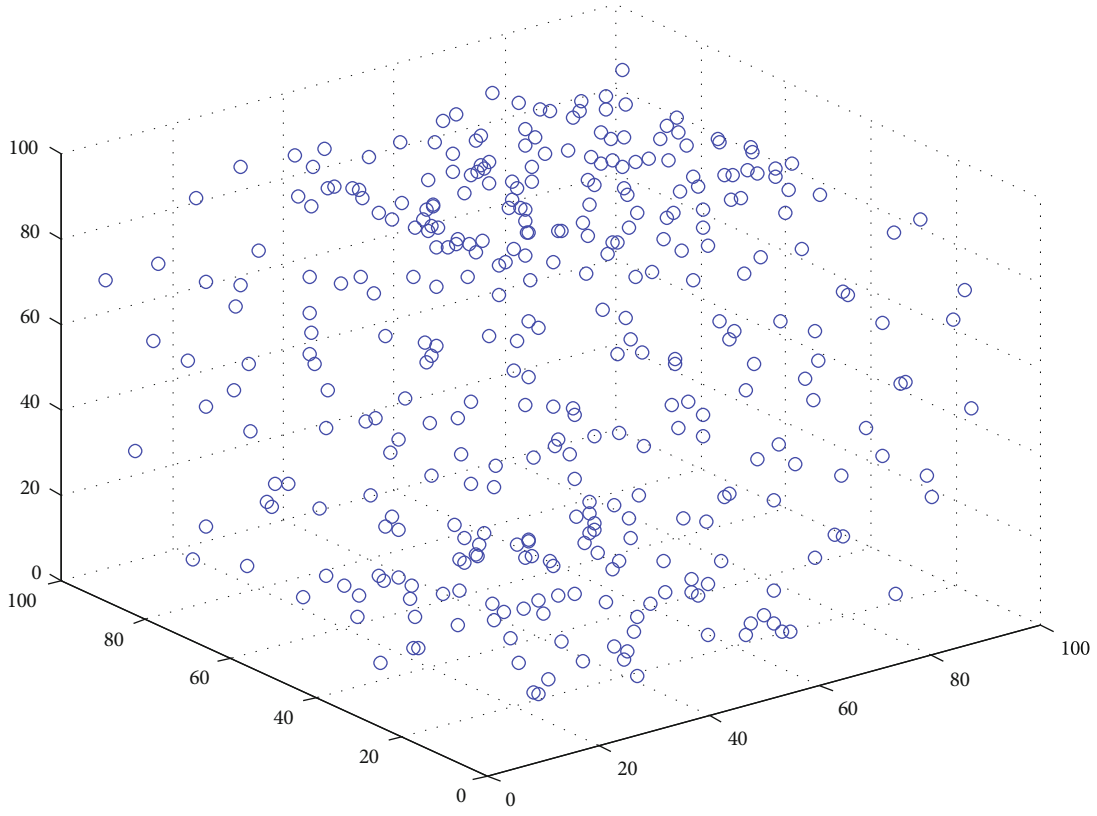

(b) After node movement

Figure 12: Coverage effect before and after node movement when the total number of nodes is 350.

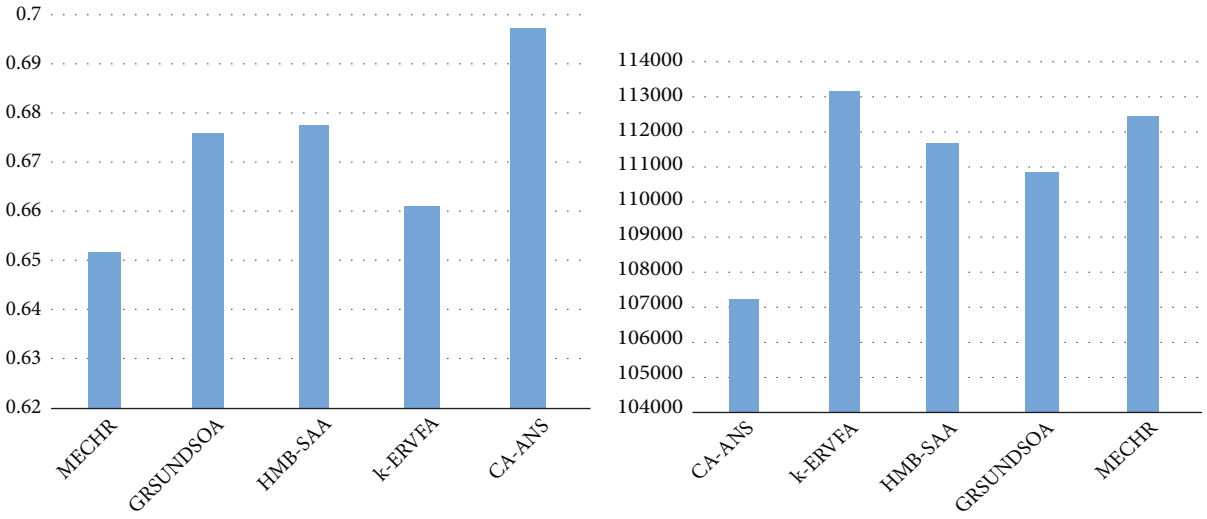

(a) Coverage effect

(b) Energy consumption

Figure 13: Coverage effect and energy consumption when the total number of nodes is 350.

$x_{new}(S_A)$ and $y_{new}(S_A)$ are the new position coordinates after the node is moved.

$x_{old}(S_A)$ and $y_{old}(S_A)$ are the original position coordinates of the node before moving.

$x_{new}(S_B)$ and $y_{new}(S_B)$ are the new position coordinates after the node is moved.

$x_{old}(S_B)$ and $y_{old}(S_B)$ are the original position coordinates of the node before moving.

In order to avoid repeated movement of nodes, each node moves only once in each cycle process. Therefore, for all nodes in the monitoring area, a set $S = \{S_1, S_2, \cdots, S_{N-1}, S_N\}$ is constructed before the beginning of each cycle, and N is the total number of nodes.

After the beginning of the tth cycle, find the sum of the two closest nodes S_A and S_B in the set. If $d(S_A, S_B) < d_t$, the cycle ends, $t = t + 1$, and enter the next cycle process. If $d(S_A, S_B) \geq d_t$, nodes move according to formulas (5) to (16). After the nodes move, delete the two nodes from the set $S = \{S_1, S_2, \cdots, S_{N-1}, S_N\}$, and find the nearest pair of nodes S_A and S_B among the remaining nodes.

It is assumed that the energy of the node S_A before moving is $E_{old}(S_A)$ and after moving is $E_{new}(S_A)$. When the energy of the node is lower than $E_{low}(S_A)$, the node does not participate in the movement and only carries out data collection and transmission; the energy of the node S_B before moving is $E_{old}(S_B)$ and after moving is $E_{new}(S_B)$. When the energy of the node is lower than $E_{low}(S_B)$, the node will not participate in the movement but only collect and transmit data.

In formulas (9) to (12), add the energy consumption module and deform the formula to obtain

$$x_{new}(S_A) = x_{old}(S_A) + d_x(S_A, S_B)\left[1 - \frac{E_{low}(S_A)}{E_{old}(S_A)}\right]\alpha, \quad (17)$$

$$y_{new}(S_A) = y_{old}(S_A) + d_y(S_A, S_B)\left[1 - \frac{E_{low}(S_A)}{E_{old}(S_A)}\right]\alpha, \quad (18)$$

$$x_{new}(S_B) = x_{old}(S_B) + d_x(S_B, S_A)\left[1 - \frac{E_{low}(S_B)}{E_{old}(S_B)}\right]\alpha, \quad (19)$$

$$y_{new}(S_B) = y_{old}(S_B) + d_y(S_B, S_A)\left[1 - \frac{E_{low}(S_B)}{E_{old}(S_B)}\right]\alpha. \quad (20)$$

In formulas (17) to (20), α is the parameter of adjusting the moving distance of the node in the process of node movement, which is related to the network environment and the characteristics of the node [32].

$$E_{new}(S_A) = E_{old}(S_A) - \beta\sqrt{[x_{new}(S_A) - x_{old}(S_A)]^2 + [y_{new}(S_A) - y_{old}(S_A)]^2}, \quad (21)$$

$$E_{new}(S_B) = E_{old}(S_B) - \beta\sqrt{[x_{new}(S_B) - x_{old}(S_B)]^2 + [y_{new}(S_B) - y_{old}(S_B)]^2}. \quad (22)$$

In formulas (21) and (22), β is the energy consumed per unit distance during node movement [33].

3.3. Buoy Sensor Node Movement Process

Step 1. Randomly deploy j buoy sensor nodes on the water surface in the monitoring area where length is L, width is W, and each sensor node has the same parameters. At this time, $t = 1$.

Step 2. Each sensor node uses the positioning function to obtain its own location and send its own location information to the sink node.

Step 3. The sink node constructs a node set $S = \{S_1, S_2, \cdots, S_{j-1}, S_j\}$ according to the location of sensor nodes in the monitoring area.

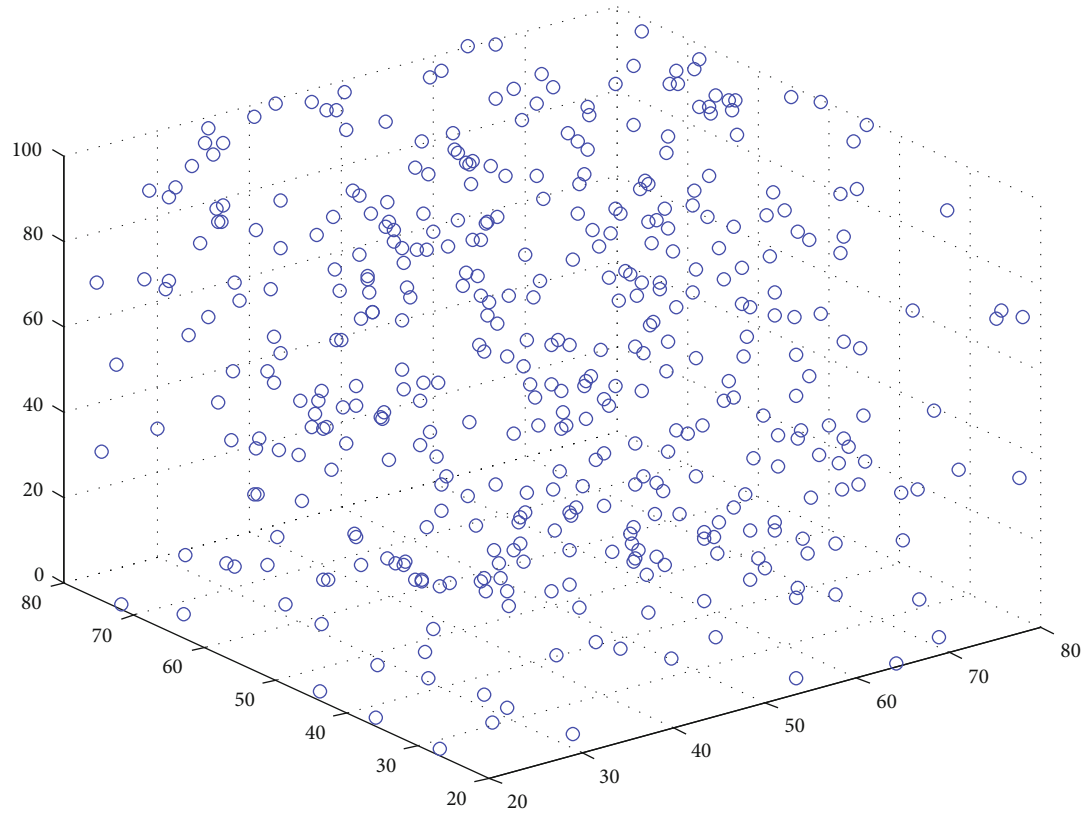

(a) Before node movement

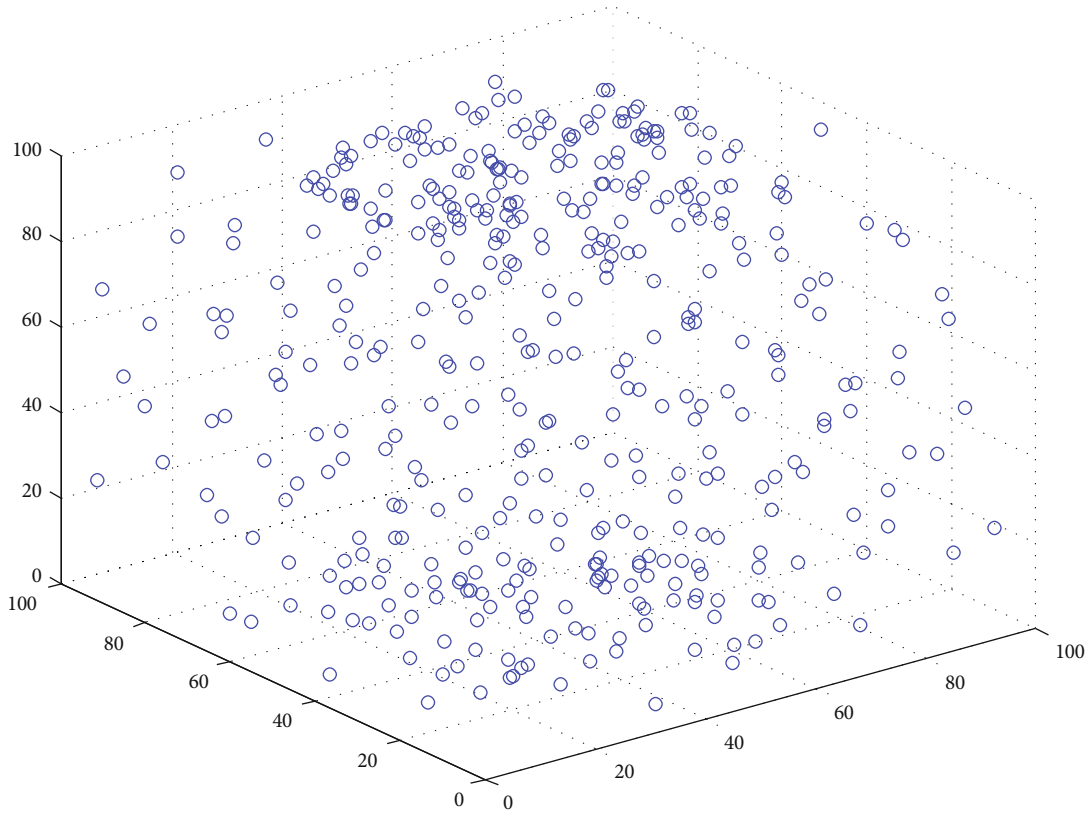

(b) After node movement

Figure 14: Coverage effect before and after node movement when the total number of nodes is 420.

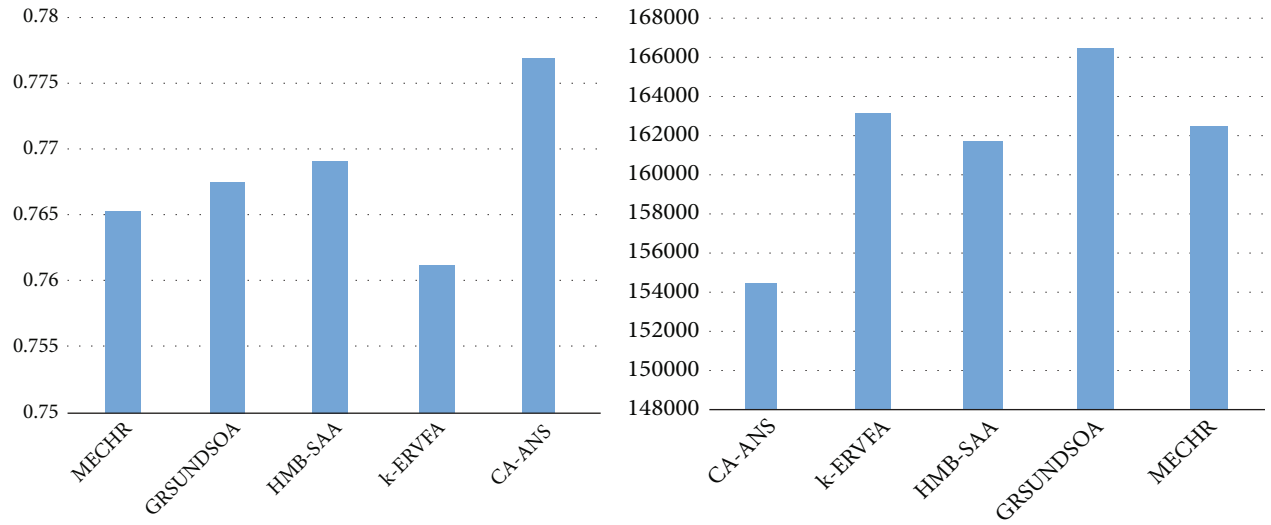

(a) Coverage effect

(b) Energy consumption

Figure 15: Coverage effect and energy consumption when the total number of nodes is 420.

Step 4. Find the two closest nodes S_A and S_B in set s.

Step 5. If $d(S_A, S_B) < d_t$, nodes move according to formulas (17) to (20).

Step 6. When any node moves outside the monitoring area, the node will not move.

Step 7. When the nodes S_A and S_B finish moving, they are removed from the set $S = \{S_1, S_2, \cdots, S_{j-1}, S_j\}$, and return to step 4.

Step 8. If $d(S_A, S_B) \geq d_t$, $t = t + 1$.

Step 9. When $t \leq T$, return to step 3 and restart the cycle process.

Step 10. When $t > T$, calculate the network coverage and residual energy of all nodes, and the algorithm ends.

3.4. Buoy Sensor Node Movement Process Pseudocode

3.5. Buoy Sensor Node Movement Process Complexity. Because step 9 returns to step 3 according to the number of cycles, the time complexity of this algorithm is determined by the number of nodes J and the number of cycles T. So the time complexity is $O(\mathrm{JT})$ in buoy sensor node movement process.

3.6. Underwater Vehicle Spacing Calculation Process. After the second type of buoy sensor is moved, the third type of underwater vehicle starts to move. Because the first type of anchor sensor and the second type of buoy sensor are not moving at this time, these two sensors can be regarded as fixed sensors, and only the third type of underwater vehicle can be moved on this basis.

According to the symmetry, the above algorithm is extended to the three-dimensional underwater network environment, and the following calculation formula is obtained.

When $d(S_A, S_B) < d_t$ the two nodes are too close, both nodes need to move.

$$d_x(S_A, S_B) = \frac{[d_t - d(S_A, S_B)](S_A^x - S_B^x)}{d(S_A, S_B)}, \tag{23}$$

$$d_y(S_A, S_B) = \frac{[d_t - d(S_A, S_B)](S_A^y - S_B^y)}{d(S_A, S_B)}, \tag{24}$$

$$d_z(S_B, S_A) = \frac{[d_t - d(S_B, S_A)](S_B^z - S_A^z)}{d(S_B, S_A)}, \tag{25}$$

$$d_x(S_B, S_A) = \frac{[d_t - d(S_B, S_A)](S_B^x - S_A^x)}{d(S_B, S_A)}, \tag{26}$$

$$d_y(S_B, S_A) = \frac{[d_t - d(S_B, S_A)](S_B^y - S_A^y)}{d(S_B, S_A)}, \tag{27}$$

$$d_z(S_B, S_A) = \frac{[d_t - d(S_B, S_A)](S_B^z - S_A^z)}{d(S_B, S_A)}. \tag{28}$$

The coordinates of the new nodes A and B are

$$x_{\mathrm{new}}(S_A) = x_{\mathrm{old}}(S_A) + d_x(S_A, S_B), \tag{29}$$

$$y_{\mathrm{new}}(S_A) = y_{\mathrm{old}}(S_A) + d_y(S_A, S_B), \tag{30}$$

$$z_{\mathrm{new}}(S_A) = z_{\mathrm{old}}(S_A) + d_z(S_A, S_B), \tag{31}$$

$$x_{\mathrm{new}}(S_B) = x_{\mathrm{old}}(S_B) + d_x(S_B, S_A), \tag{32}$$

$$y_{\mathrm{new}}(S_B) = y_{\mathrm{old}}(S_B) + d_y(S_B, S_A), \tag{33}$$

$$z_{\mathrm{new}}(S_B) = z_{\mathrm{old}}(S_B) + d_z(S_B, S_A). \tag{34}$$

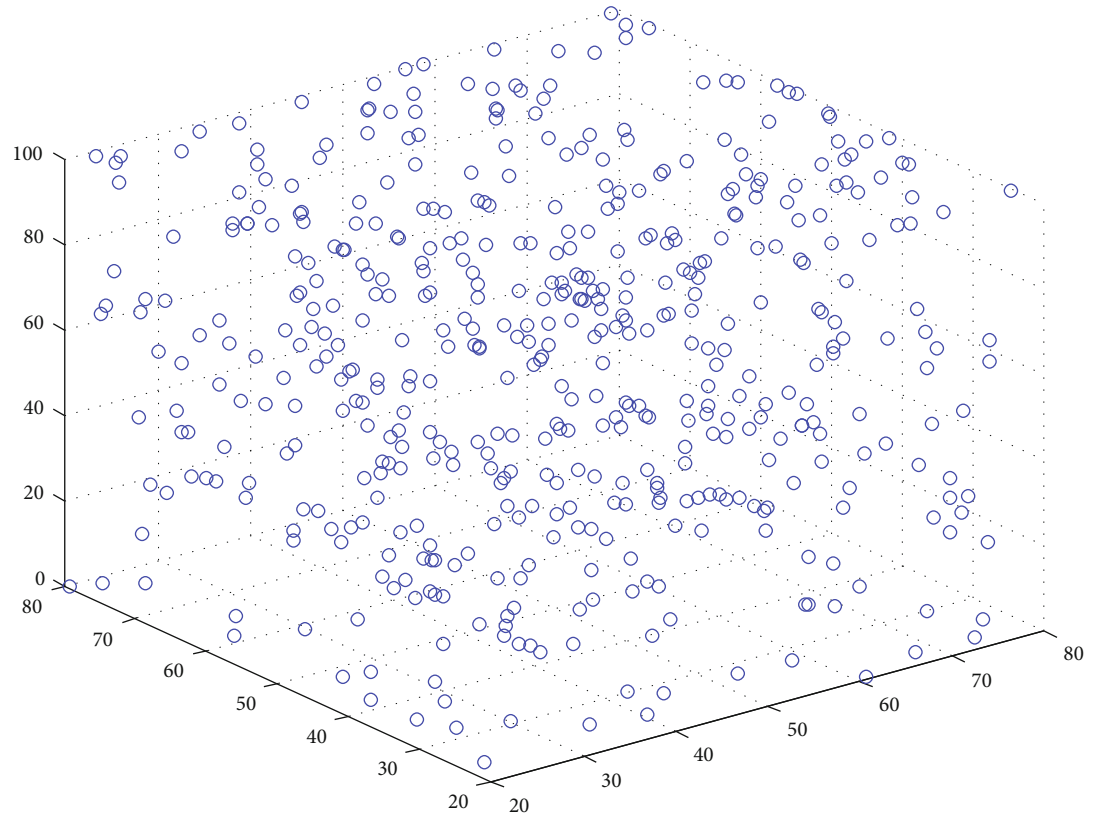

(a) Before node movement

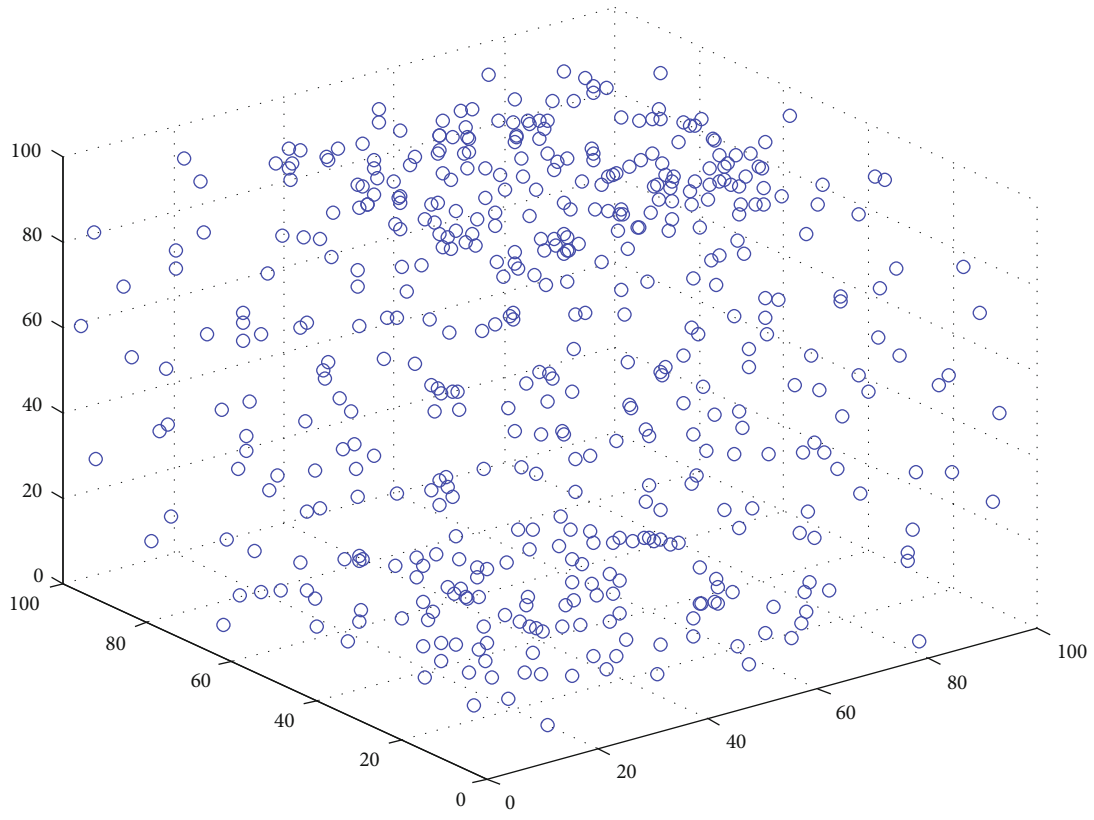

(b) After node movement

Figure 16: Coverage effect before and after node movement when the total number of nodes is 490.

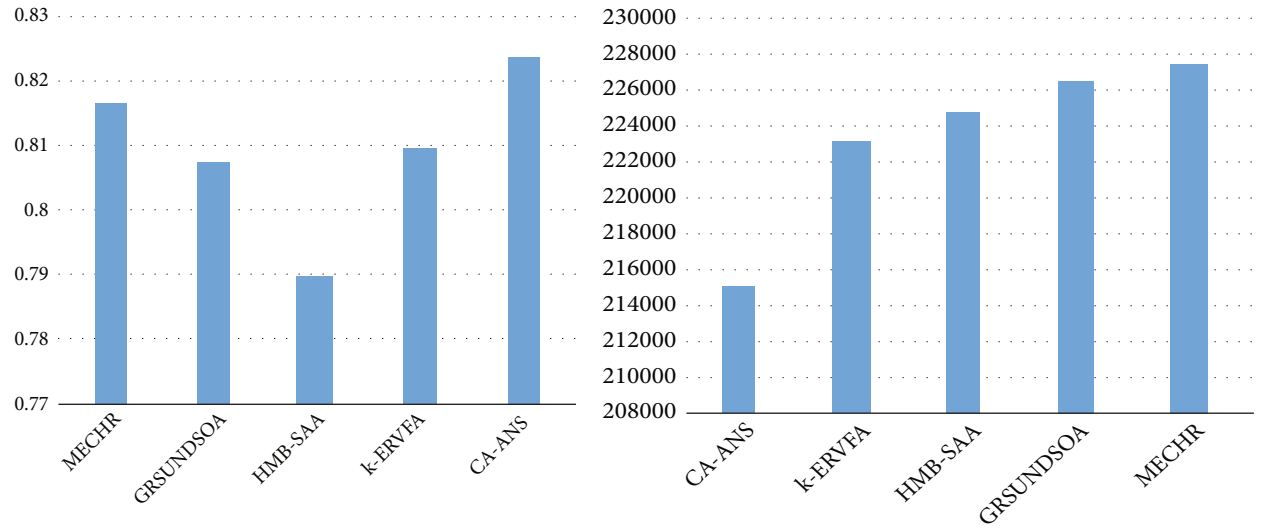

(a) Coverage effect

(b) Energy consumption

Figure 17: Coverage effect and energy consumption when the total number of nodes is 490.

When $d(S_A, S_B) \geq d_t$,

$$x_{\text{new}}(S_A) = x_{\text{old}}(S_A), \tag{35}$$

$$y_{\text{new}}(S_A) = y_{\text{old}}(S_A), \tag{36}$$

$$z_{\text{new}}(S_A) = z_{\text{old}}(S_A), \tag{37}$$

$$x_{\text{new}}(S_B) = x_{\text{old}}(S_B), \tag{38}$$

$$y_{\text{new}}(S_B) = y_{\text{old}}(S_B), \tag{39}$$

$$z_{\text{new}}(S_B) = z_{\text{old}}(S_B). \tag{40}$$

In formulas (23) to (34), $d_x(S_A, S_B)$ is that node A obtains the displacement component along the x-axis from node B.

$d_y(S_A, S_B)$ is that node A obtains the displacement component along the y-axis from node B.

$d_z(S_A, S_B)$ is that node A obtains the displacement component along the z-axis from node B.

$d_x(S_B, S_A)$ is that node B obtains the displacement component along the x-axis from node A.

$d_y(S_B, S_A)$ is that node B obtains the displacement component along the y-axis from node A.

$d_z(S_B, S_A)$ is that node B obtains the displacement component along the z-axis from node A.

d_t is the ideal distance between nodes in the tth cycle.

$d(S_A, S_B)$ is the distance between node A and node B.

$d(S_B, S_A)$ is the distance between node B and node A.

S_A^x is the position coordinates of node A on the x-axis.

S_A^y is the position coordinates of node A on the y-axis.

S_A^z is the position coordinates of node A on the z-axis.

S_B^x is the position coordinates of node B on the x-axis.

S_B^y is the position coordinates of node B on the y-axis.

S_B^z is the position coordinates of node B on the z-axis.

$x_{\text{new}}(S_A)$, $y_{\text{new}}(S_A)$, and $z_{\text{new}}(S_A)$ are the new position coordinates after the node is moved.

$x_{\text{old}}(S_A)$, $y_{\text{old}}(S_A)$, and $z_{\text{old}}(S_A)$ are the original position coordinates of the node before moving.

$x_{\text{new}}(S_B)$, $y_{\text{new}}(S_B)$, and $z_{\text{new}}(S_B)$ are the new position coordinates after the node is moved.

$x_{\text{old}}(S_B)$, $y_{\text{old}}(S_B)$, and $z_{\text{old}}(S_B)$ are the original position coordinates of the node before moving.

In order to avoid repeated movement of nodes, each node moves only once in each cycle process. Therefore, for all nodes in the monitoring area, a set $S = \{S_1, S_2, \cdots, S_{N-1}, S_N\}$ is constructed before the beginning of each cycle, and N is the total number of nodes.

After the beginning of the tth cycle, find the sum of the two closest nodes S_A and S_B in the set $S = \{S_1, S_2, \cdots, S_{N-1}, S_N\}$. If $d(S_A, S_B) \leq d_t$, the cycle ends, $t = t + 1$. Start to enter the next cycle process. If $d(S_A, S_B) > d_t$, nodes move according to formulas (5) to (22). After the nodes move, delete the two nodes from the set $S = \{S_1, S_2, \cdots, S_{N-1}, S_N\}$, and find the next pair of nearest nodes S_A and S_B in the remaining nodes.

It is assumed that the energy of the node S_A before moving is $E_{\text{old}}(S_A)$ and after moving is $E_{\text{new}}(S_A)$. When the energy of the node is lower than $E_{\text{low}}(S_A)$, the node does not participate in the movement and only carries out data collection and transmission; the energy of the node S_B before moving is $E_{\text{old}}(S_B)$ and after moving is $E_{\text{new}}(S_B)$. When the energy of the node is lower than $E_{\text{low}}(S_B)$, the node will not participate in the movement but only collect and transmit data.

In formulas (29) to (34), add the energy consumption module and deform the formula to obtain

$$x_{\text{new}}(S_A) = x_{\text{old}}(S_A) + d_x(S_A, S_B)\left[1 - \frac{E_{\text{low}}(S_A)}{E_{\text{old}}(S_A)}\right]\alpha, \tag{41}$$

$$y_{\text{new}}(S_A) = y_{\text{old}}(S_A) + d_y(S_A, S_B)\left[1 - \frac{E_{\text{low}}(S_A)}{E_{\text{old}}(S_A)}\right]\alpha, \tag{42}$$

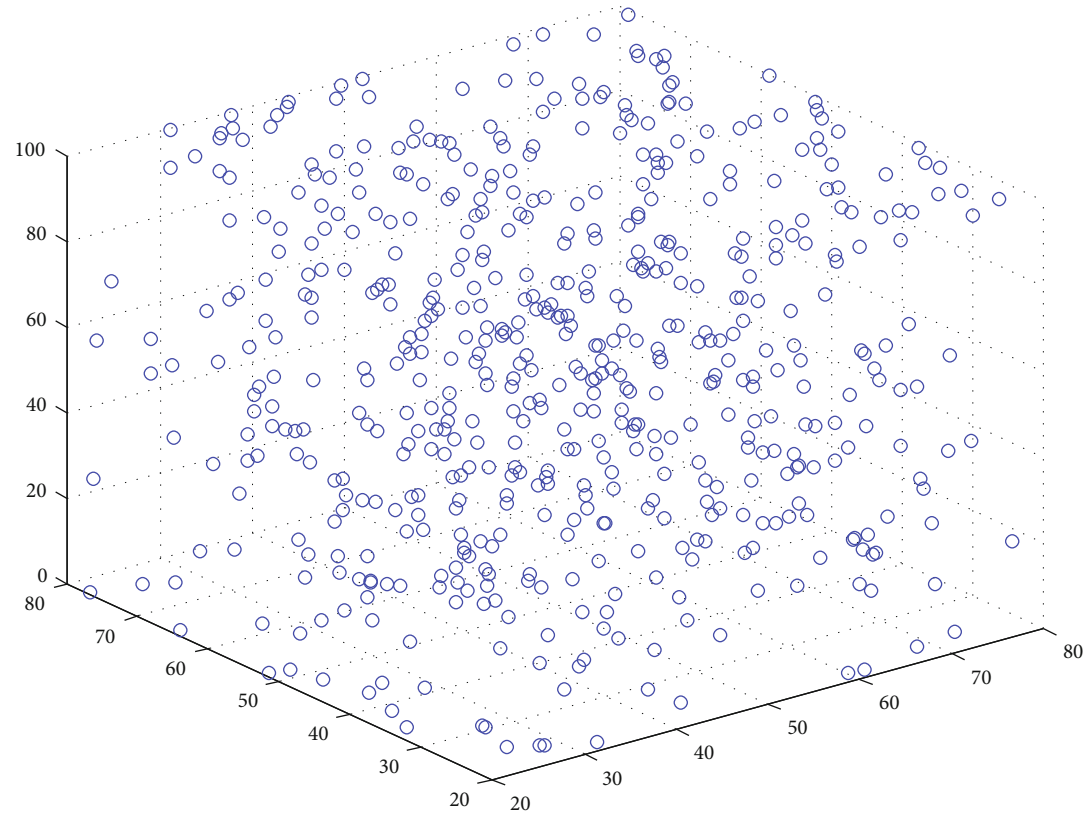

(a) Before node movement

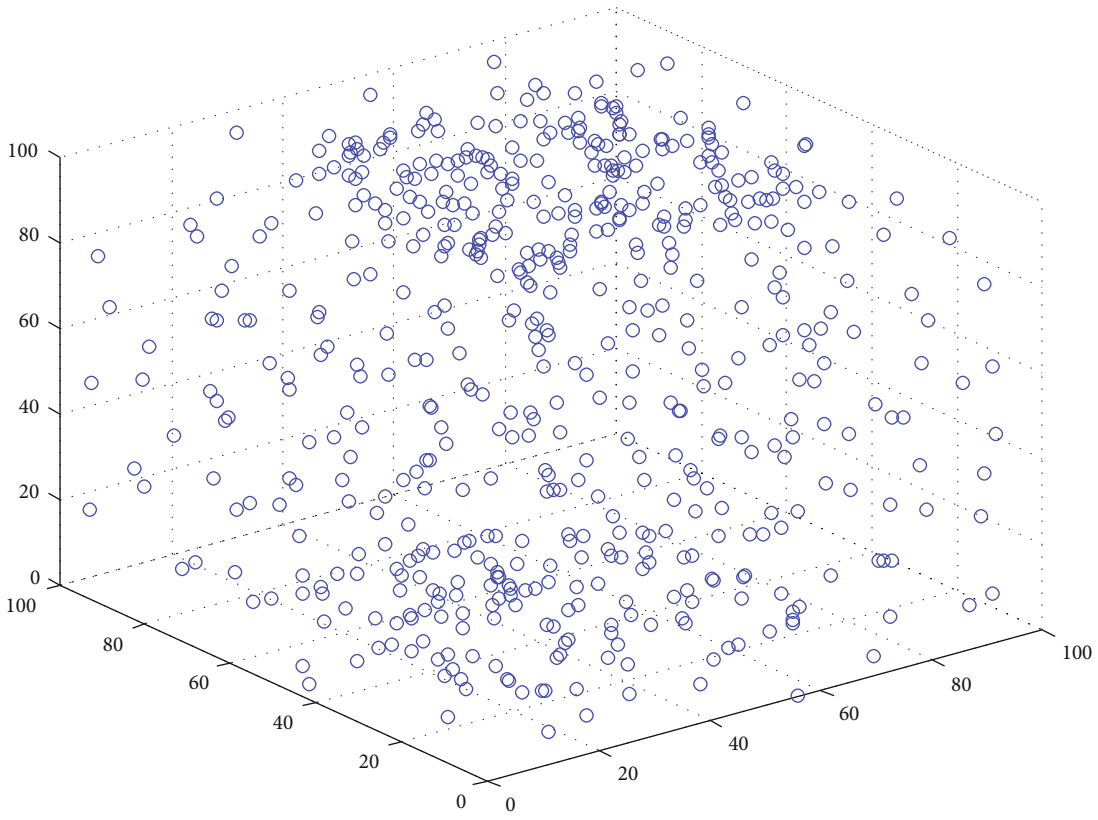

(b) After node movement

Figure 18: Coverage effect before and after node movement when the total number of nodes is 560.

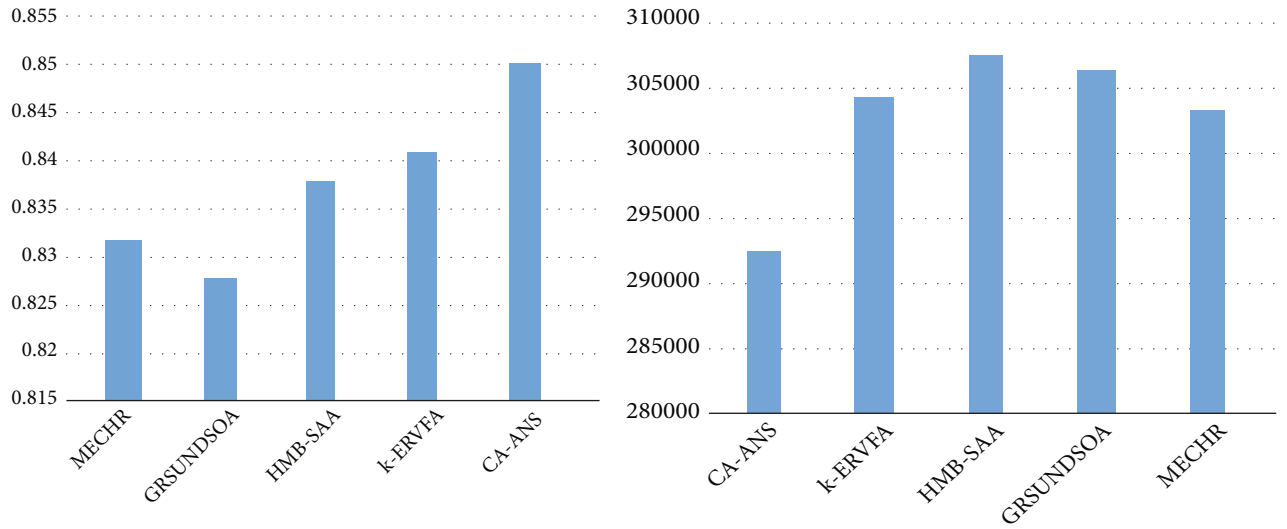

(a) Coverage effect

(b) Energy consumption

Figure 19: Coverage effect and energy consumption when the total number of nodes is 560.

$$z_{\text{new}}(S_A) = z_{\text{old}}(S_A) + d_z(S_A, S_B)\left[1 - \frac{E_{\text{low}}(S_A)}{E_{\text{old}}(S_A)}\right]\alpha, \quad (43)$$

$$x_{\text{new}}(S_B) = x_{\text{old}}(S_B) + d_x(S_B, S_A)\left[1 - \frac{E_{\text{low}}(S_B)}{E_{\text{old}}(S_B)}\right]\alpha, \quad (44)$$

$$y_{\text{new}}(S_B) = y_{\text{old}}(S_B) + d_y(S_B, S_A)\left[1 - \frac{E_{\text{low}}(S_B)}{E_{\text{old}}(S_B)}\right]\alpha, \quad (45)$$

$$z_{\text{new}}(S_B) = z_{\text{old}}(S_B) + d_z(S_B, S_A)\left[1 - \frac{E_{\text{low}}(S_B)}{E_{\text{old}}(S_B)}\right]\alpha. \quad (46)$$

In formulas (41) to (46), α is the parameter of adjusting the moving distance of the node in the process of node movement, which is related to the network environment and the characteristics of the node [34].

$$E_{\text{new}}(S_A) = E_{\text{old}}(S_A) - \beta\sqrt{[x_{\text{new}}(S_A) - x_{\text{old}}(S_A)]^2 + [y_{\text{new}}(S_A) - y_{\text{old}}(S_A)]^2 + [z_{\text{new}}(S_A) - z_{\text{old}}(S_A)]^2}, \quad (47)$$

$$E_{\text{new}}(S_B) = E_{\text{old}}(S_B) - \beta\sqrt{[x_{\text{new}}(S_B) - x_{\text{old}}(S_B)]^2 + [y_{\text{new}}(S_B) - y_{\text{old}}(S_B)]^2 + [z_{\text{new}}(S_B) - z_{\text{old}}(S_B)]^2}. \quad (48)$$

In formulas (47) and (48), β is the energy consumed per unit distance during node movement [35].

3.7. Underwater Vehicle Node Movement Process

Step 1. Randomly deploy k underwater vehicles in the monitoring area where length is L, width is W, and depth is D. At this time, $t = 1$.

Step 2. After deployment, each sensor node uses the positioning function to obtain its own location and send its own location information to the sink node.

Step 3. The sink node constructs a node set $S = \{S_1, S_2, \cdots, S_{k-1}, S_k\}$ according to the location of k underwater vehicle nodes in the monitoring area and finds the two closest nodes S_A and S_B in the set s.

Step 4. If $d(S_A, S_B) < d_t$, nodes move according to formulas (23) to (28).

Step 5. If any node is moved outside the monitoring area after the movement, the node will not move.

Step 6. Remove the two nodes S_A and S_B from the set $S = \{S_1, S_2, \cdots, S_{k-1}, S_k\}$.

Step 7. Find the next pair of two nearest nodes S_A and S_B in the remaining nodes of set s, and return to step 4.

Step 8. If $d(S_A, S_B) \geq d_t$, $t = t + 1$.

Step 9. When $t \leq T$, go to step 3 and restart the cycle process.

Step 10. When $t > T$, calculate the network coverage and residual energy of all nodes, and the algorithm ends.

3.8. Underwater Vehicle Node Movement Process Pseudocode

3.9. Underwater Vehicle Node Movement Process Complexity.

Because step 9 returns to step 3 according to the number of cycles, the time complexity of the entire algorithm is determined by the number of nodes K and the number of cycles T. So the time complexity is $O(\text{KT})$ in underwater vehicle node movement process.

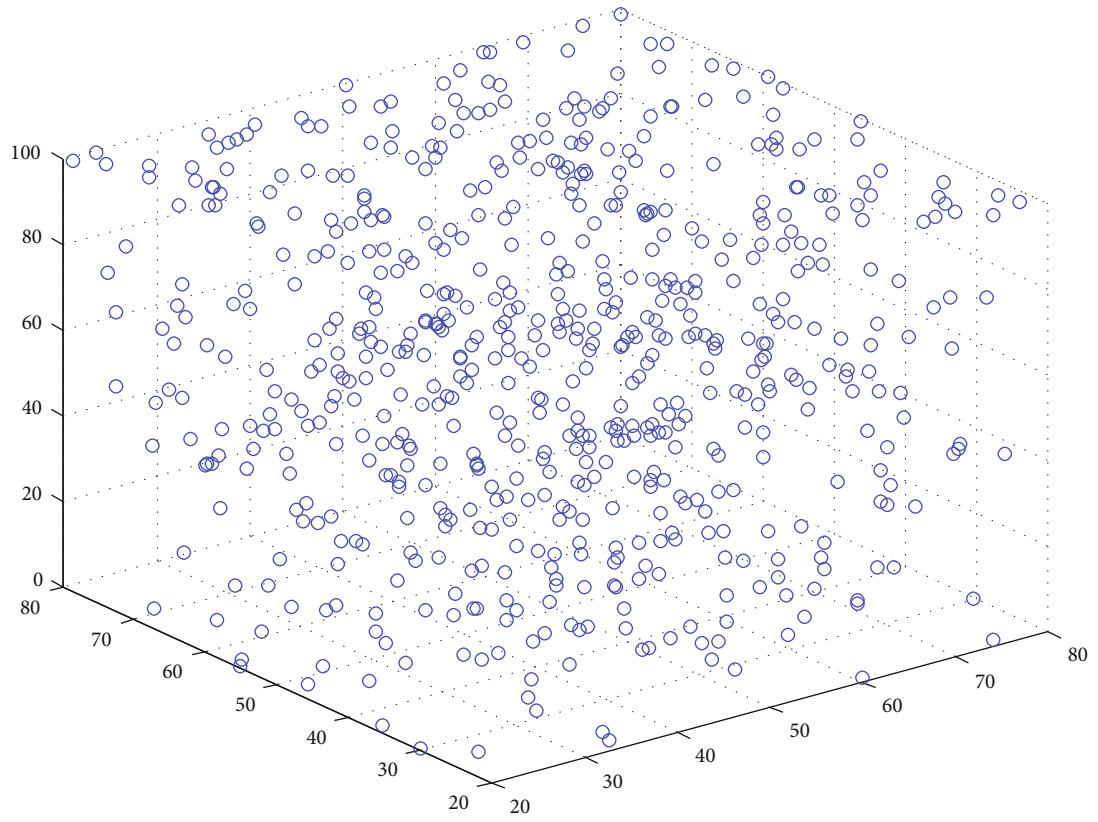

(a) Before node movement

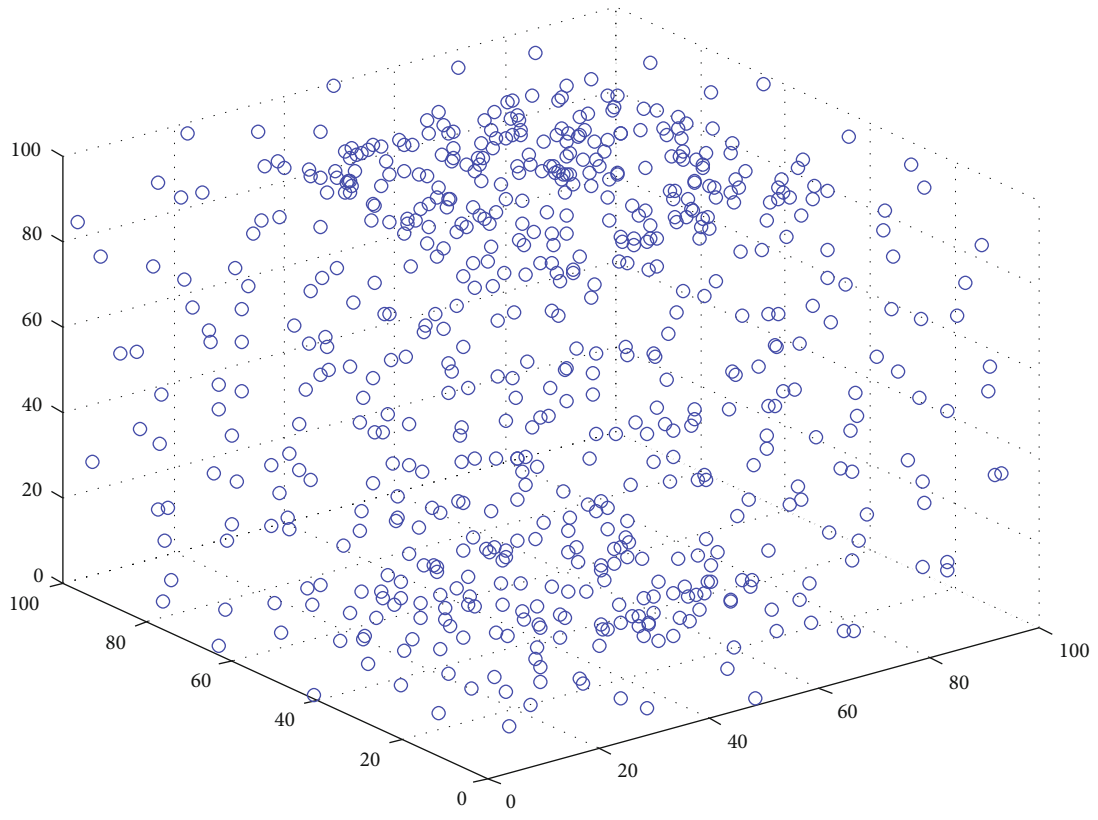

(b) After node movement

Figure 20: Coverage effect before and after node movement when the total number of nodes is 630.

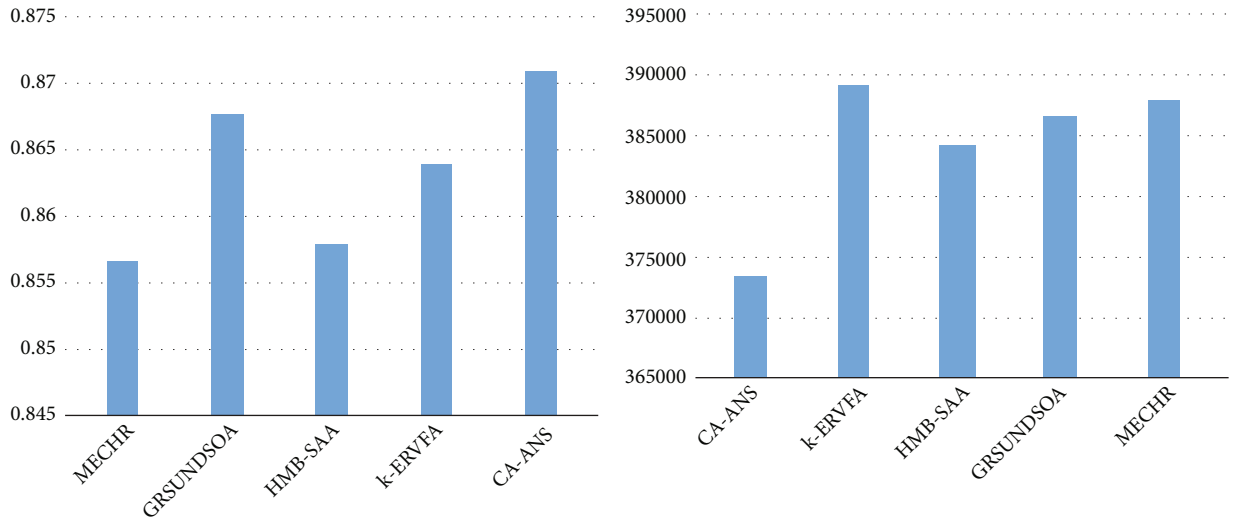

(a) Coverage effect

(b) Energy consumption

Figure 21: Coverage effect and energy consumption when the total number of nodes is 630.

4. Simulation Analysis

In this article, software is used for simulation verification, and the relevant parameters are as follows.

The length of the monitoring area $L = 100$ m, width of the monitoring area $W = 100$ m, depth of the monitoring area $d = 100$ m, node communication radius $R_C = 20$ m, node sensing radius $R_S = 10$ m, parameter $\alpha = 1$, parameter $\beta = 10$, node initial energy $E_{\text{initial}}(S) = 100000$ J, node movable minimum energy $E_{\text{low}}(S) = 10000$ J, cycle times $T = 20$, and $d_t = (1 + (t/T)) \times R_S$.

In order to verify the effectiveness of this algorithm, under the same parameter conditions, CA-ANS algorithm is compared with MECHR algorithm, GRSUNDSOA algorithm, HMB-SAA algorithm, and K-ERVFA algorithm.

Because the anchor sensor cannot be moved after deployment, if it is widely used, the coverage effect of the monitoring area will not be significantly improved. Although the buoy sensor can move, its moving range is limited and it can only move on the water. Therefore, after a large number of deployment, it can only improve the coverage effect in a limited range. The underwater vehicle that can move freely can move according to the monitoring needs. If it is reasonably deployed after extensive use, it can quickly and effectively improve the coverage effect of the monitoring area.

When the number of anchored sensors $i = 10$, 20, 30, 40, 50, 60, 70, 80, and 90; the number of buoy sensors $j = 20$, 40, 60, 80, 100, 120, 140, 160, and 180; and the number of underwater vehicles $k = 40$, 80, 120, 160, 200, 240, 280, 320, and 360, the simulation is carried out to compare the coverage effect and energy consumption of wireless sensor nodes after moving. The data set provided by reference [36] is used for simulation. The simulation results are shown in Figures 4–21. In order to better observe the displacement effect before and after node movement, this article uses three-dimensional view to explain.

(1) When $i = 10$, $j = 20$, and $k = 40$

(2) When $i = 20$, $j = 40$, and $k = 80$

(3) When $i = 30$, $j = 60$, and $k = 120$

(4) When $i = 40$, $j = 80$, and $k = 160$

(5) When $i = 50$, $j = 100$, and $k = 200$

(6) When $i = 60$, $j = 120$, and $k = 240$

(7) When $i = 70$, $j = 140$, and $k = 280$

(8) When $i = 80$, $j = 160$, and $k = 320$

(9) When $i = 90$, $j = 180$, and $k = 360$

From Figures 4–21, it can be seen that with the increase of the number of nodes, the network coverage and node energy consumption under different algorithms increase. This algorithm adjusts the distance between nodes and considers the energy consumption of nodes. In the process of node movement, for the node with less residual energy,

reduce its moving distance to avoid its failure due to energy consumption. Therefore, the coverage algorithm based on adjusting the node spacing proposed in this article can effectively improve the network coverage and reduce the energy consumption of nodes in the network. At the same time, the distance between nodes is gradually increased, avoiding the situation of invalid round-trip movement.

5. Conclusion

In order to solve the coverage problem of 3D underwater wireless sensor network, an underwater wireless sensor network coverage algorithm based on adjusting the node spacing is proposed in this article. The algorithm uses three different types of nodes. By reasonably adjusting the distance between nodes, the nodes in the dense area are gradually dispersed, so as to achieve the goal of improving the effective coverage area of the monitoring area. The reasonable distance between nodes is calculated before each cycle, and the distance between nodes is gradually increased, which can avoid the invalid movement of nodes and reduce unnecessary movement of nodes. The simulation results show that the algorithm improves the coverage of wireless sensor networks and reduces the energy consumption of wireless sensor nodes.

Data Availability

The data used to support the findings of this research are available from the corresponding authors upon request.

Conflicts of Interest

The authors declare that there are no conflicts of interest.

Acknowledgments

This research was supported in part by the National Natural Science Foundation of China (No. 61375021) and NUAA Fundamental Research Funds for the Central Universities (No. 3082020NZ2020017).

References

[1] K. D. Praveen, A. Tarachand, and A. C. S. Rao, "Machine learning algorithms for wireless sensor networks: a survey," *Information Fusion*, vol. 49, pp. 1–25, 2019.

[2] F. Jie and C. Fangjiong, "Data reconstruction coverage based on graph signal processing for wireless sensor networks," *IEEE Wireless Communications Letters*, vol. 11, no. 1, pp. 48–52, 2022.

[3] S. C. Wang, H. C. Hsiao, C. C. Lin, and H. H. Chin, "Multi-objective wireless sensor network deployment problem with cooperative distance-based sensing coverage," *Mobile Networks and Applications*, vol. 27, no. 1, pp. 3–14, 2022.

[4] J. Feng, H. Chen, X. Deng, L. T. Yang, and F. Tan, "Confident information coverage hole prediction and repairing for healthcare big data collection in large-scale hybrid wireless sensor networks," *IEEE Internet of Things Journal*, vol. 8, no. 23, pp. 16801–16813, 2021.

[5] C. Aparajita and D. Debashis, "Energy-efficient coverage optimization in wireless sensor networks based on Voronoi-Glowworm Swarm Optimization-K-means algorithm," *Ad Hoc Networks*, vol. 122, article 102660, 2021.

[6] H. Yu, C. Y. Chang, Y. Wang, D. S. Roy, and X. Bai, "CAERM: coverage aware energy replenishment mechanism using mobile charger in wireless sensor networks," *IEEE Sensors Journal*, vol. 21, no. 20, pp. 23682–23697, 2021.

[7] C. Liu and H. Du, "T, K-sweep coverage with mobile sensor nodes in wireless sensor networks," *IEEE Internet of Things Journal*, vol. 8, no. 18, pp. 13888–13899, 2021.

[8] R. Ghazalian, A. Aghagolzadeh, and S. M. H. Andargoli, "Energy optimization of wireless visual sensor networks with the consideration of the desired target coverage," *IEEE Transactions on Mobile Computing*, vol. 20, no. 9, pp. 2795–2807, 2021.

[9] H. M. Ammari, "Connected _k_ -coverage in two-dimensional wireless sensor networks using hexagonal slicing and area stretching," *Journal of Parallel and Distributed Computing*, vol. 153, no. 10, pp. 89–109, 2021.

[10] H. Wu, Q. Li, H. Zhu, X. Han, Y. Li, and B. Yang, "Directional sensor placement in vegetable greenhouse for maximizing target coverage without occlusion," *Wireless Networks*, vol. 26, no. 6, pp. 4677–4687, 2020.

[11] P. Singh and Y. C. Chen, "Sensing coverage hole identification and coverage hole healing methods for wireless sensor networks," *Wireless Networks*, vol. 26, no. 3, pp. 2223–2239, 2020.

[12] F. Hajjej, M. Hamdi, R. Ejbali, and M. Zaied, "A distributed coverage hole recovery approach based on reinforcement learning for wireless sensor networks," *Ad Hoc Networks*, vol. 101, article 102082, 2020.

[13] C. Zygowski and A. Jaekel, "Optimal path planning strategies for monitoring coverage holes in wireless sensor networks," *Ad Hoc Networks*, vol. 96, article 101990, 2020.

[14] K.-B. Saeed, G. Jun, and J. Hamid, "Energy-efficient node deployment in heterogeneous two-tier wireless sensor networks with limited communication range," *IEEE Transactions on Wireless Communications*, vol. 20, no. 1, pp. 40–55, 2021.

[15] E. Levent, "Point coverage with heterogeneous sensor networks: a robust optimization approach under target location uncertainty," *Computer Networks*, vol. 198, article 108416, 2021.

[16] R. R. Priyadarshini and N. Sivakumar, "Enhancing coverage and connectivity using energy prediction method in underwater acoustic WSN," *Journal of Ambient Intelligence and Humanized Computing*, vol. 11, no. 7, pp. 2751–2760, 2020.

[17] Y. Zhuang, C. Wu, H. Wu et al., "Event coverage hole repair algorithm based on multi-AUVs in multi-constrained three-dimensional underwater wireless sensor networks," *Symmetry-Basel*, vol. 12, no. 11, p. 1884, 2020.

[18] R. Priyadarshi and B. Gupta, "Area coverage optimization in three-dimensional wireless sensor network," *Wireless Personal Communications*, vol. 117, no. 2, pp. 843–865, 2020.

[19] L. Yao and X. Du, "Sensor coverage strategy in underwater wireless sensor networks," *International Journal of Computers Communications and Control*, vol. 15, no. 2, p. 3659, 2020.

[20] L. Yan, Y. He, and Z. Huangfu, "An uneven node self-deployment optimization algorithm for maximized coverage and energy balance in underwater wireless sensor networks," *Sensors*, vol. 21, no. 4, p. 1368, 2021.

[21] W. Zhang, G. Han, Y. Liu, and J. Wang, "A coverage vulnerability repair algorithm based on clustering in underwater wireless sensor networks," *Mobile Networks and Applications*, vol. 26, no. 3, pp. 1107–1121, 2020.

[22] W. Shen, C. Zhang, and J. Shi, "Weak k-barrier coverage problem in underwater wireless sensor networks," *Mobile Networks and Applications*, vol. 24, no. 5, pp. 1526–1541, 2019.

[23] L. Liu, J. Du, and Y. Liu, "Topology control for diverse coverage in underwater wireless sensor networks," *ACM Transactions on Autonomous and Adaptive Systems*, vol. 11, no. 3, p. 16, 2016.

[24] K. Latif, N. Javaid, A. Ahmad, Z. A. Khan, N. Alrajeh, and M. I. Khan, "On energy hole and coverage hole avoidance in underwater wireless sensor networks," *IEEE Sensors Journal*, vol. 16, no. 11, pp. 4431–4442, 2016.

[25] D. N. Sandeep and V. Kumar, "Review on clustering, coverage and connectivity in underwater wireless sensor networks: a communication techniques perspective," *Access*, vol. 5, pp. 11176–11199, 2017.

[26] W. Wang, H. Huang, F. He, F. Xiao, X. Jiang, and C. Sha, "An enhanced virtual force algorithm for diverse k-coverage deployment of 3D underwater wireless sensor networks," *Sensors*, vol. 19, no. 16, p. 3496, 2019.

[27] S. W. Li, D. Q. Ma, Q. Y. Li, J. W. Zhang, and X. Zhang, "Nodes deployment algorithm based on perceived probability of heterogeneous wireless sensor network," in *International Conference on Advanced Mechatronic Systems, ICAMechS*, pp. 374–378, Luoyang, China, 2013.

[28] N. Wu, J. Zhang, Q. Li et al., "Mobile nodes deployment scheme design based on perceived probability model in heterogeneous wireless sensor network," *Journal of Robotics and Mechatronics*, vol. 26, no. 5, pp. 616–621, 2014.

[29] J. Zhang, S. Li, Q. Li, Y. Liu, and N. Wu, "Coverage hole recovery algorithm based on perceived probability in heterogeneous wireless sensor network," *The Journal of Computer Information Systems*, vol. 10, no. 7, pp. 2983–2990, 2014.

[30] Q. Li and N. Liu, "Monitoring area coverage optimization algorithm based on nodes perceptual mathematical model in wireless sensor networks," *Computer Communications*, vol. 155, pp. 227–234, 2020.

[31] L. Qiangyi and L. Ningzhong, "Nodes deployment algorithm based on data fusion and evidence theory in wireless sensor networks," *Wireless Personal Communications*, vol. 116, no. 2, pp. 1481–1492, 2021.

[32] Q. Li and N. Liu, "Coverage optimization algorithm based on control nodes position in wireless sensor networks," *International Journal of Communication Systems*, vol. 35, no. 5, 2022.

[33] Q. Li and N. Liu, "Coverage blind area repair based on perceived multimedia data driven in mobile wireless sensor networks," *Advances in Multimedia*, vol. 2022, Article ID 2354024, 10 pages, 2022.

[34] Q. Li and N. Liu, "Monitoring area coverage based on control multimedia nodes position in mixed underwater mobile wireless sensor networks," *Advances in Multimedia*, vol. 2022, Article ID 5888728, 10 pages, 2022.

[35] Q. Li and N. Liu, "Monitoring area coverage based on improved virtual force and multimedia nodes movement data in mobile wireless sensor networks," *Advances in Multimedia*, vol. 2022, Article ID 7121469, 9 pages, 2022.

[36] D. K. Sah, K. Cengiz, P. K. Donta, V. N. Inukollu, and T. Amgoth, "EDGF: empirical dataset generation framework for wireless sensor networks," *Computer Communications*, vol. 180, pp. 48–56, 2021.